

OPEN ACCESS

**Repository of the Max Delbrück Center for Molecular Medicine (MDC)
in the Helmholtz Association**

<https://edoc.mdc-berlin.de/18680>

**DLC1 is a direct target of activated YAP/TAZ that drives collective
migration and sprouting angiogenesis.**

van der Stoel M., Schimmel L., Nawaz K., van Stalborch A.M., de Haan A., Klaus-Bergmann A., Valent E.T., Koenis D.S., van Nieuw Amerongen G.P., de Vries C.J., de Waard V., Gloerich M., van Buul J.D., Huveneers S.

This is a copy of the final article, which is published here by [permission of the publisher](#) and which appeared first in final edited form in:

Journal of Cell Science
2020 FEB 12 ; 133(3): jcs239947
doi: [10.1242/jcs.239947](https://doi.org/10.1242/jcs.239947)
Publisher: [The Company of Biologists Ltd.](#)

Copyright © 2020. Published by The Company of Biologists Ltd.
<http://www.biologists.com/user-licence-1-1/>

RESEARCH ARTICLE

DLC1 is a direct target of activated YAP/TAZ that drives collective migration and sprouting angiogenesis

Miesje van der Stoel¹, Lilian Schimmel², Kalim Nawaz², Anne-Marieke van Stalborch², Annett de Haan¹, Alexandra Klaus-Bergmann^{3,4}, Erik T. Valent⁵, Duco S. Koenis¹, Geerten P. van Nieuw Amerongen⁵, Charlie J. de Vries¹, Vivian de Waard¹, Martijn Gloerich⁶, Jaap D. van Buul^{2,7} and Stephan Huveneers^{1,*}

ABSTRACT

Endothelial YAP/TAZ (YAP is also known as YAP1, and TAZ as WWTR1) signaling is crucial for sprouting angiogenesis and vascular homeostasis. However, the underlying molecular mechanisms that explain how YAP/TAZ control the vasculature remain unclear. This study reveals that the focal adhesion protein deleted-in-liver-cancer 1 (DLC1) is a direct transcriptional target of the activated YAP/TAZ-TEAD complex. We find that substrate stiffening and VEGF stimuli promote expression of DLC1 in endothelial cells. In turn, DLC1 expression levels are YAP and TAZ dependent, and constitutive activation of YAP is sufficient to drive DLC1 expression. DLC1 is needed to limit F-actin fiber formation, integrin-based focal adhesion lifetime and integrin-mediated traction forces. Depletion of endothelial DLC1 strongly perturbs cell polarization in directed collective migration and inhibits the formation of angiogenic sprouts. Importantly, ectopic expression of DLC1 is sufficient to restore migration and angiogenic sprouting in YAP-depleted cells. Together, these findings point towards a crucial and prominent role for DLC1 in YAP/TAZ-driven endothelial adhesion remodeling and collective migration during angiogenesis.

This article has an associated First Person interview with the first author of the paper.

KEY WORDS: Mechanotransduction, Endothelium, Adhesion, Integrin, YAP, Angiogenesis

INTRODUCTION

The formation of new blood and lymphatic vessels through angiogenesis is essential for development and vital for tissue regeneration and tumorigenesis (Gomez-Salinerio and Rafii, 2018; Potente et al., 2011). The luminal side of the vasculature is covered by a well-organized layer of endothelial cells. Angiogenesis is

driven by endothelial cell proliferation and migration, during which the endothelial cells coordinate their movements collectively through remodeling of interactions with the vascular microenvironment and contacts between the endothelial cells (Betz et al., 2016; Szymborska and Gerhardt, 2018).

The yes-associated protein (YAP, also known as YAP1) and transcriptional co-activator with PDZ-binding motif (TAZ or WWTR1) proteins are key molecular switches that shuttle between the cytoplasm and nucleus to control proliferation and migration (Panciera et al., 2017). Several studies have demonstrated the importance of YAP/TAZ for angiogenesis and vascular homeostasis (Choi et al., 2015; Nakajima et al., 2017; Wang et al., 2016a, 2017; Neto et al., 2018). Mechanical cues, such as extracellular matrix (ECM) stiffness and shear stress, control the activity of YAP/TAZ (Dupont, 2016) and are important tissue properties that guide angiogenesis (Dorland and Huveneers, 2017; Choi et al., 2015; Nakajima et al., 2017; Wang et al., 2016a, 2017; Neto et al., 2018). In addition, angiogenic signaling through vascular endothelial growth factor (VEGF) promotes activation of YAP/TAZ and a migratory transcriptional program to support developmental angiogenesis (Wang et al., 2017). YAP and TAZ activation is further regulated by Rho GTPase signaling and cytoskeletal contractility (Dupont et al., 2011; Elosegui-Artola et al., 2017).

Inactive YAP and TAZ are localized in the cytoplasm, whereas active YAP and TAZ (i.e. upon ECM stiffening, disturbed flow or sparse cell densities) translocate to the nucleus (Dupont et al., 2011). Nuclear YAP/TAZ act as co-activators of TEA domain family members (TEAD) transcription factors to promote vascular development (Vassilev et al., 2001; Astone et al., 2018). Recently, it was shown that YAP/TAZ activation is needed to provide transcriptional feedback for collective migration of endothelial cells (Mason et al., 2019). Strikingly, the transcriptional target(s) of YAP/TAZ that are responsible for endothelial migration in angiogenesis remain to be identified.

We previously observed that deleted-in-liver-cancer 1 (DLC1, also known as STARD12 or ARHGAP7) expression is high in endothelial cells on stiff substrates (Schimmel et al., 2018), pointing towards a putative downstream role for DLC1 in YAP/TAZ signaling. DLC1 is crucial for embryonic development and its depletion in mice leads to severe defects of various organs at embryonic day (E)10.5 (Durkin et al., 2005). DLC1 is an endothelial-enriched GTPase-activating protein (GAP) that inactivates Rho GTPases (van Buul et al., 2014). In addition, DLC1 has a serine-rich region that contains binding motifs for components of integrin-based focal adhesions (Barras and Widmann, 2014; Kim et al., 2009). Focal adhesions are crucial structures for mechanotransduction and migration, as they connect cells to the ECM and mechanically couple the contractile actin cytoskeleton to the extracellular microenvironment (Geiger et al., 2001; Gardel et al., 2010; Grashoff et al., 2010).

¹Amsterdam UMC, University of Amsterdam, location AMC, Department of Medical Biochemistry, Amsterdam Cardiovascular Sciences, 1105 AZ Amsterdam, The Netherlands. ²Sanquin Research and Landsteiner Laboratory, Department of Molecular and Cellular Hemostasis, University of Amsterdam, 1066 CX Amsterdam, The Netherlands. ³Max-Delbrück-Center for Molecular Medicine, Robert-Rössle-Strasse 10, 13125 Berlin, Germany. ⁴DZHK (German Center for Cardiovascular Research), 10785 Berlin, Germany. ⁵Amsterdam UMC, Free University, location VUMC, Department of Physiology, Amsterdam Cardiovascular Sciences, 1081 HV Amsterdam, The Netherlands. ⁶University Medical Center Utrecht, Center for Molecular Medicine, Dept. Molecular Cancer Research, 3584 CX Utrecht, The Netherlands. ⁷Leeuwenhoek Centre for Advanced Microscopy (LCAM), section Molecular Cytology at Swammerdam Institute for Life Sciences (SILS) at University of Amsterdam, 1098 XH Amsterdam, The Netherlands.

*Author for correspondence (s.huveneers@amsterdamumc.nl)

© E.T.V., 0000-0002-1640-0119; G.P.v.N.A., 0000-0002-4307-3029; J.D.v.B., 0000-0003-0054-7949; S.H., 0000-0002-1091-475X

In this study, we identify DLC1 as a novel transcriptional target of the activated YAP/TAZ–TEAD complex. Expression of DLC1 is needed for integrin-based focal adhesion disassembly, cell polarization, collective cell migration and angiogenic sprouting. We further demonstrate that ectopic expression of DLC1 in YAP-depleted endothelial cells restores their migration and angiogenic sprouting capacity. In conclusion, we demonstrate that DLC1 is a crucial transcriptional target of YAP/TAZ in the endothelium. These findings place DLC1 as a key player in YAP/TAZ signaling and likely has wider implications for YAP/TAZ-driven flow sensing and the development of stiffness-related vascular diseases.

RESULTS

DLC1 is a transcriptional target of YAP/TAZ and TEAD

We recently showed that DLC1 protein expression is high within stiff microenvironments of the vasculature (Schimmel et al., 2018). To investigate if varying substrate stiffness directly controls DLC1 expression, primary human umbilical vein endothelial cells (HUVECs) were cultured on fibronectin-coated 2 kPa (soft), 50 kPa (intermediate stiffness) and plastic (stiff) substrates. Western blot analysis of HUVEC lysates demonstrated elevated DLC1 protein levels on stiffer substrates (Fig. 1A). To study whether DLC1 upregulation in stiff microenvironments occurs through transcriptional upregulation we performed quantitative PCR (qPCR) on RNA isolations from HUVECs. These experiments showed that mRNA levels of DLC1 are increased on stiff substrates (Fig. 1B). To investigate how DLC1 transcription is controlled by stiffness, we explored the promoter region of the DLC1 gene. We found a TEAD-binding motif (CATTCCA) close to the transcriptional start site of the predominant DLC1 transcript variant expressed in endothelial cells (transcript variant 2, encoding for a 123 kDa protein). Analysis of publicly available TEAD1 chromatin immunoprecipitation sequencing data sets showed that TEAD1 binds this particular motif in a variety of different cell types (Fig. 1C; Fig. S1). To study whether the TEAD-binding motif in the promoter region of DLC1 transcript variant 2 regulates promoter activity, wild-type or a TEAD binding motif-mutated variant of the promoter region of DLC1 (−418 to +319 bp) was fused to a luciferase reporter gene in a transient expression plasmid. Since transfections were inefficient in the primary HUVECs, luciferase activity was monitored in lysates of transfected HEK cells cultured on plastic (stiff) substrates, which showed that mutating the TEAD motif perturbed transcriptional activation of the DLC1 promoter (Fig. 1D). Because YAP and TAZ act as co-factors for the TEAD family of transcription factors (Vassilev et al., 2001; Astone et al., 2018), we next investigated whether YAP or TAZ are responsible for stiffness-induced DLC1 expression in endothelial cells. We performed short hairpin RNA (shRNA)-based knockdowns of YAP and TAZ in HUVECs cultured on plastic (stiff) substrates. Western blot analysis showed a strong reduction in the expression of DLC1 upon knockdown of YAP or TAZ (Fig. 1E,F), as well as the known YAP/TAZ–TEAD target connective tissue growth factor (CTGF, also known as CCN2) (Zhao et al., 2008).

To establish whether activation of YAP/TAZ through other upstream cues might control DLC1 expression levels, serum and growth factor-starved HUVECs were treated with VEGF for 2 h. Indeed, the VEGF treatments readily activated YAP, as analyzed by reduced phosphorylation of its serine 127 as reported previously (Wang et al., 2017), and upregulated expression levels of DLC1 (Fig. 1G). Next, a constitutive nuclear YAP-5SA mutant that cannot be inactivated by the LATS1 and LATS2 (LATS1/2) kinases of the

Hippo pathway (Zhao et al., 2007), was expressed in HUVECs. Expression of YAP-5SA strongly upregulated DLC1 and CTGF expression in HUVECs cultured on plastic substrates (Fig. 1H). To investigate whether the constitutively active YAP-induced expression of DLC1 depends on substrate stiffness, control and YAP-5SA-expressing HUVECs were cultured on 2 kPa substrates. Western blot analysis demonstrated that YAP-5SA efficiently promoted DLC1 expression even on soft substrates (Fig. 1I). Overall, these results demonstrate that DLC1 is a transcriptional target of YAP/TAZ and TEAD in the endothelium, and that YAP activation is sufficient to drive DLC1 expression.

DLC1 controls endothelial focal adhesion turnover and traction forces

To investigate the role of DLC1 downstream of YAP/TAZ in the endothelium, we silenced DLC1 expression through shRNAs. Three of the five tested shRNA plasmids induced efficient knockdown of DLC1 protein levels in HUVECs (Fig. 2A) and shDLC1 plasmids #1063 and/or #1064 were used for follow-up experiments. DLC1 might function at cadherin-based cell–cell junctions and integrin-based focal adhesions (Tripathi et al., 2012; Zacharchenko et al., 2016; Qian et al., 2007). DLC1 knockdown resulted in the formation of prominent basal F-actin fibers in endothelial cells, while the cells maintained their VE-cadherin-based cell–cell junctions (Fig. 2B). As YAP/TAZ are required for VE-cadherin dynamics and cell–cell junction formation in the vasculature (Neto et al., 2018), we first investigated the role of DLC1 in endothelial barrier function by performing electric cell–substrate impedance sensing (ECIS). Upon knockdown of DLC1, no significant changes were detected in endothelial barrier formation and maintenance of the barrier in time (Fig. 2C). Since DLC1 is a GAP for Rho GTPases (Kim et al., 2009), we next compared the GTP-loading of RhoA in lysates of shControl- and shDLC1-expressing HUVECs by means of G-LISA. We detected no differences in either basal or thrombin-stimulated RhoA activity levels between shControl and shDLC1 cells (Fig. 2D). These data indicate that endothelial DLC1 is not required for the formation of endothelial cell–cell junctions, barrier function or RhoA activation.

Lentiviral expression of an N-terminal GFP-tagged DLC1 (Qian et al., 2007) showed that DLC1 is recruited to focal adhesions in HUVECs (Fig. 2E). Next, we investigated the role of DLC1 at endothelial integrin-based adhesions by immunofluorescence staining for paxillin in shControl- and shDLC1-expressing HUVECs. These experiments showed that depletion of DLC1 strongly increased the number of focal adhesions that were connected to prominent F-actin fibers (Fig. 2F). Integrin-based focal adhesions are highly dynamic structures, and are constantly being formed and disassembled (Möhl et al., 2012; Geiger et al., 2009; Gardel et al., 2010). To decipher the mechanism underlying the remodeling of focal adhesions mediated by DLC1, we performed live imaging using total internal reflection fluorescence microscopy (TIRF) of shControl and shDLC1 HUVECs expressing mCherry-tagged paxillin. Consistent with our above findings, the TIRF imaging showed that DLC1-depleted HUVECs contained more focal adhesions (Fig. 2G; Movie 1; note only ~10–20% of the cell population in the monolayer is paxillin–mCherry positive). Overall, the change in adhesion turnover in the absence of DLC1 resulted in a striking stabilization of the focal adhesions (Fig. 2G, pseudocolored focal adhesions in right panels). Quantitative analysis using established focal adhesion-tracking software (Berginski and Gomez, 2013) showed an increase in focal adhesion lifetime, which corresponded with a decrease in focal

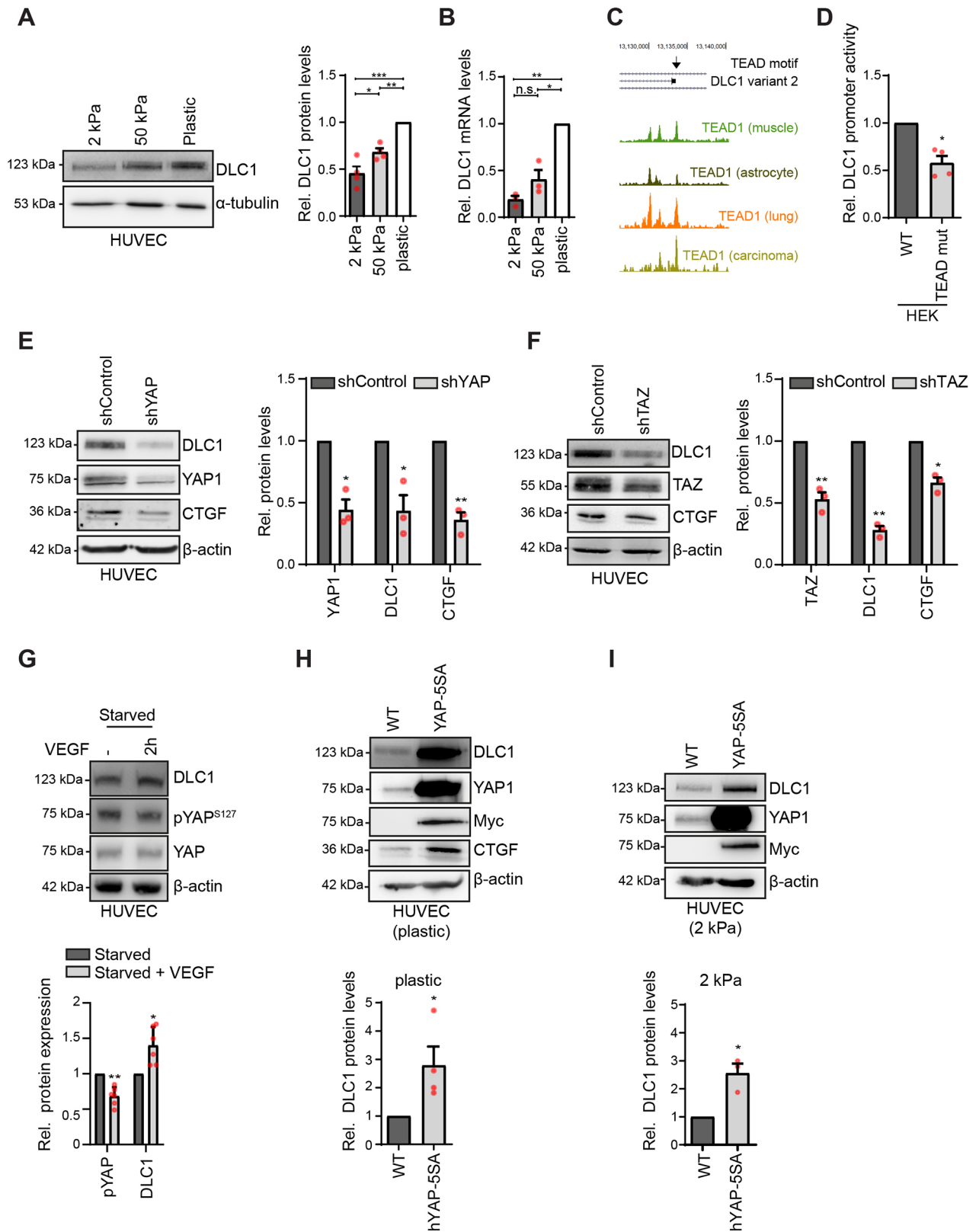


Fig. 1. See next page for legend.

adhesion disassembly rates, while assembly rates remained comparable (Fig. 2H). To investigate the functional consequences of depletion of DLC1 for force transduction from cells to the ECM, traction force microscopy (TFM) was performed using

shControl- and shDLC1-expressing HUVECs. These experiments demonstrated that depletion of DLC1 promoted endothelial traction forces throughout the monolayer, and strongly raised the root mean square of exerted traction forces (Fig. 2I). Thus, DLC1 expression is

Fig. 1. DLC1 is a transcriptional target of YAP/TAZ and TEAD.

(A) Representative western blot analysis of DLC1 and α -tubulin (loading control) in total lysates of HUVECs cultured on fibronectin-coated 2 kPa or 50 kPa hydrogels, or plastic. Graph shows the mean \pm s.e.m. protein expression levels. Signal has been corrected for background and relative to expression in HUVECs on plastic. Data from four independent experiments. * P <0.05; ** P <0.01; *** P <0.001 (one-way ANOVA and Dunnett's post-test). (B) qPCR analysis of DLC1 mRNA isolated from HUVECs cultured on fibronectin-coated 2 kPa or 50 kPa hydrogels, or plastic. Graph shows the mean \pm s.e.m. gene expression levels. Values are normalized to expression levels of the housekeeping gene RPLP0, and are presented relative to mRNA expression levels in HUVECs on plastic. Data from three independent experiments. * P <0.05; ** P <0.01; n.s., not significant (one-way ANOVA and Dunnett's post-test). (C) Schematics of UCSC genome browser results at position chr8:13,074,715-13,142,890 of the human genome (GRCh38/hg38) displaying the genomic location of DLC1 transcript variants 1 (NP872584.2), 2 (NP.006085.2) and 5 (NP.001303597.1) and the presence of a TEAD motif at the transcriptional start site of DLC1 transcript variant 2. Plotted are the results from publicly available GEO TEAD1 ChIP-Seq data (Table S1) from various cell types. The data show a binding peak of TEAD1 at the transcription start site (TSS) of DLC1 isoform 2. See Fig. S1 for more details, including histone modification and DNase hypersensitivity profiles of the promoter region in HUVECs. (D) Graph shows the mean \pm s.e.m. relative promoter activity of DLC1 in lysates of HEK cells transfected with the wild-type (WT) human DLC1 promoter region (from the -418 to +319 bp position relative to the TSS of DLC1 isoform 2) fused to a firefly luciferase reporter or a DLC1 promoter luciferase reporter in which the TEAD-binding motif was mutated from CATTCCA to AGACTAT. Firefly luciferase activities of the TEAD mutated promoter were corrected for co-transfected *Renilla* luciferase activity and normalized to WT promoter activity. Data are from four independent experiments. * P <0.05 (paired Student's *t*-test). (E,F) Representative western blot analysis of DLC1 in total lysates of HUVECs transduced with shControl, shYAP (E) or shTAZ (F). Graph shows the mean \pm s.e.m. protein expression level signal corrected for background and normalized to expression in shControl-transduced HUVECs. Data from three independent experiments. * P <0.05, ** P <0.01 (paired Student's *t*-test). (G) Representative western blot analysis of DLC1, YAP phosphorylated at serine 127 (pYAP^{S127}), YAP1 and β -actin (loading control) in total cell lysate samples of starved non-stimulated HUVECs (-) or starved HUVECs stimulated with 1 mg/ml VEGF for 2 h. Graph shows the mean \pm s.e.m. protein expression level signal corrected for background and normalized to expression in non-transduced HUVECs. Data from six independent experiments. * P <0.05, ** P <0.01 (paired Student's *t*-test). (H) Representative western blot analysis of DLC1, YAP1, Myc, CTGF and β -actin (loading control) in total lysates of non-transduced HUVECs (WT) and HUVECs transduced with Myc-tagged human YAP-5SA. Graph shows the mean \pm s.e.m. protein expression level signal corrected for background and normalized to expression in non-transduced HUVECs. Data from four independent experiments. * P <0.05 (paired Student's *t*-test). (I) Representative western blot analysis of DLC1, YAP1, Myc and β -actin (loading control) in total lysates of non-transduced HUVECs (WT) and HUVECs transduced with Myc-tagged human YAP-5SA cultured on 2 kPa hydrogels. Graph shows the mean \pm s.e.m. protein expression level signal corrected for background and normalized to expression in non-transduced HUVECs. Data from three independent experiments. * P <0.05 (paired Student's *t*-test). Scans of whole western blots are depicted in Fig. S2.

driven by substrate stiffness, and in turn, expression of DLC1 controls force transduction at the cell-ECM interface. Together, the data show that DLC1 is needed for efficient turnover of endothelial focal adhesions and traction forces.

Endothelial DLC1 controls cell orientation and directed migration

In cell collectives, YAP/TAZ translocate to the nuclei of leader cells to regulate endothelial cell migration (Lin et al., 2017; Yu and Guan, 2013; Zhang et al., 2015; Mason et al., 2019; Neto et al., 2018) (see also Fig. S3). We next examined whether endothelial DLC1 is involved in collective cell migration. Knockdown of DLC1 strongly inhibited endothelial migration in scratch wound assays (Fig. 3A-C;

Movie 2), supporting previous findings for a role of DLC1 in migration of prostate epithelial cells (Shih et al., 2012). Within 12 h, control monolayers closed on average 88.89% of the wound area, while DLC1 knockdown inhibited scratch wound closure (41.66% and 67.16% for an shRNA targeting the 3' UTR of DLC1 mRNA and clone #1063 respectively; Fig. 3B,C). No changes in cell proliferation were observed between the conditions (Fig. 3D), indicating that the delay in wound healing was due to migration defects. To investigate how DLC1 controls cell dynamics, we performed tracking of individual endothelial cells within the confluent monolayers in time-lapse experiments. Whereas control cells migrated collectively in a persistent fashion in the direction of wound closure, DLC1-depleted cells lost their capability for directional migration (Fig. 3E; Movie 2). These data demonstrate that DLC1 coordinates collective cell migration.

Cell polarization is needed for persistent migration, and is characterized by the orientation of the Golgi in front of the nucleus (Kupfer et al., 1982; Bisel et al., 2013). To study whether DLC1 controls cell polarization during migration, shControl- and shDLC1-expressing endothelial monolayers were analyzed 6 h after the initiation of scratch wound migration. Golgi orientation was determined in the first three leader cell rows in immunostainings for GM130 (also known as GOLGA2, a Golgi marker). In control HUVECs, 60% of the cells oriented their Golgi in the direction of migration, whereas only 23% to 37% of DLC1-depleted cells were polarized (Fig. 3F). To decipher the importance of DLC1 in the establishment of polarized leader cells, we performed a competition scratch assay. We generated mosaic endothelial monolayers in which half of the population of HUVECs expressed shControl with a RFP tag or HUVECs expressing the shDLC1 3'UTR and GFP. Next, scratch assays were performed and the identity of the leader cells during collective migration was determined at $t=0$ and $t=12$ h after scratching. The experiments demonstrated that the leading front is predominantly formed by cells that express DLC1, whereas DLC1-depleted cells failed to lead during the collective cell migration process (Fig. 3G; Movie 3). To investigate whether the failure of DLC1 knockdown cells to lead collective migration relates to differences in focal adhesion turnover, we investigated the alignment of focal adhesions in leader cells 6 h after the onset of migration. Immunostainings for vinculin, a marker of focal adhesions, showed that, in the absence of DLC1, the focal adhesions aligned more among each other than in control cells, but the aligned focal adhesions oriented perpendicularly ($>90^\circ$ dominant angle) to the direction of scratch wound closure (Fig. 3H). Overall, these results clearly show that DLC1 is needed for endothelial cell polarization and focal adhesion organization during collective cell migration.

DLC1 is required for sprouting angiogenesis

Directional migration of endothelial cells is essential for sprouting angiogenesis (Lamallice et al., 2007; Eilken and Adams, 2010; Franco et al., 2015). Moreover, the sensing of ECM stiffness and exertion of tensional forces occurs through endothelial integrin-based adhesions and directs the formation of angiogenic sprouts (Fischer et al., 2019; Korff and Augustin, 1999). To establish whether DLC1 plays a role in angiogenic sprouting, shControl and shDLC1 HUVECs were cultured in spheroids and placed in 3D collagen matrices to assess sprouting capacity as described previously (Heiss et al., 2015; Martin et al., 2018). Subsequently, sprouting was induced by treatment with VEGF. Visualization of sprout formation after 16 h, showed a decrease in cumulative length and the number of sprouts after depletion of DLC1 (Fig. 4A).

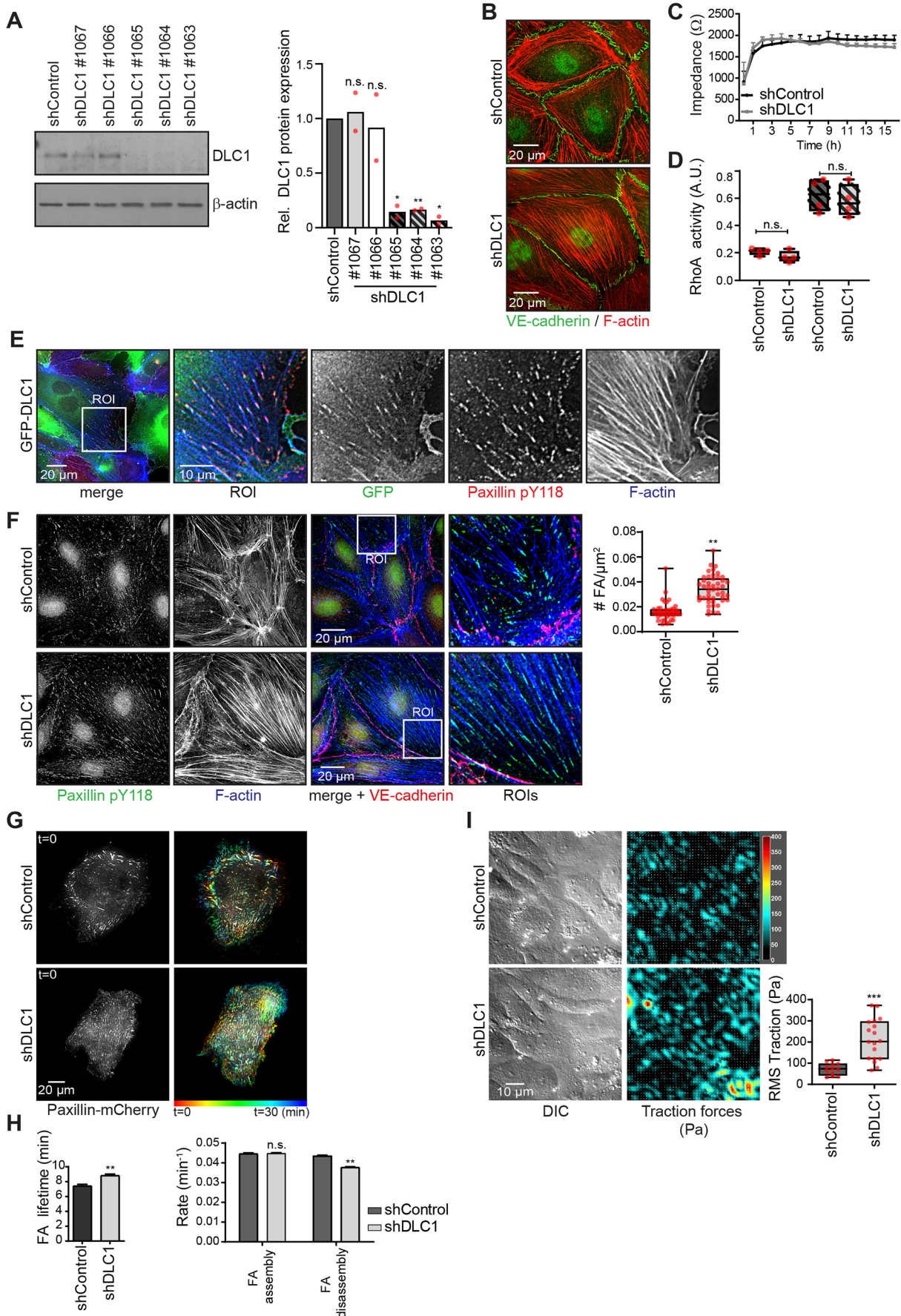


Fig. 2. See next page for legend.

Fig. 2. DLC1 controls endothelial focal adhesion turnover and traction forces. (A) Representative western blot analysis of DLC1 and β -actin (loading control) in total lysates of HUVECs transduced with different shDLC1 clones (#1067, #1066, #1065, #1064 and #1063). Graph shows the mean. DLC1 protein expression level signal corrected for background and normalized to expression in shControl-transduced HUVECs. Data from two independent experiments. * $P < 0.05$; ** $P < 0.01$; n.s., not significant (paired Student's *t*-test). (B) Widefield immunofluorescence images of HUVECs transduced with shControl or shDLC1 (pool of #1063 and #1064) and stained for VE-cadherin (green) and F-actin (red). (C) Line graph shows the mean \pm s.d. transendothelial impedance measured at 4000 Hz across barrier-forming endothelial cells transduced with shControl or shDLC1 (pool of #1063 and #1064) plated on fibronectin-coated 8W10E ECIS arrays. Representative data are from two independent experiments and an average of six wells per condition. (D) Box-plot showing quantification of RhoA activity in G-LISA assays in lysates of shControl and shDLC1-transduced HUVECs, with or without thrombin stimulation. Whiskers show the range. Data are from four independent experiments. A.U., arbitrary units. n.s., not significant (two-tailed unpaired Student's *t*-test). (E) Representative widefield immunofluorescence images of HUVECs transduced with GFP–DLC1 stained for Paxillin pY118 (red) and F-actin (blue). (F) Widefield immunofluorescence images of shControl- and shDLC1-transduced HUVECs stained for paxillin pY118 (green), F-actin (blue) and VE-cadherin (red). Box-plot showing quantification of manually counted number of focal adhesions (FAs) per μm^2 of shControl- and shDLC1-transduced HUVECs. Whiskers show the range. Data are from two independent experiments, shControl (42 cells from 12 images) and shDLC1 (46 cells from 19 images). ** $P < 0.01$ (two-tailed unpaired Student's *t*-test). (G) Left images are stills from time-lapse TIRF microscopy at $t=0$ of HUVECs transduced with shControl or shDLC1, and paxillin–mCherry. Heat map in the right panels shows the corresponding focal adhesion dynamics over 30 min in a unique color per time frame. Note the stability of focal adhesions in shDLC1 HUVECs. See corresponding Movie 1 for the ~ 2.5 h time-lapse recording. (H) Bar graphs showing quantification of focal adhesion lifetime, assembly and disassembly rates based on TIRF time-lapse experiments with paxillin–mCherry-expressing HUVECs. Error bars are s.e.m. Data are from two independent experiments; shControl (six movies, more than 4000 tracked focal adhesions) and shDLC1 (eight movies, more than 6000 tracked focal adhesions). Focal adhesion tracking was performed using the focal adhesion analysis webserver (Berginski and Gomez, 2013). ** $P < 0.01$; n.s., not significant (two-tailed unpaired Student's *t*-test). (I) DIC images and cell–substrate traction force maps of HUVECs transduced with shControl or shDLC1. Box-plot showing the median (and upper and lower quartiles) of measured RMS traction forces of shControl (12 image fields) and shDLC1 (18 image fields) endothelial cells. Whiskers show the range. Data are from three independent experiments. *** $P < 0.001$ (two-tailed unpaired Student's *t*-test).

Moreover, overexpression of GFP–DLC1 efficiently promoted sprout formation compared to GFP-transduced control HUVECs (Fig. 4B). These data indicate that expression levels of DLC1 determine angiogenic sprouting efficiency. To verify the contribution of DLC1 in sprouting angiogenesis, we first depleted endogenous DLC1 by mean of shRNAs targeting the 3' UTR of the mRNA. Subsequently, GFP or GFP–DLC1, which are not targeted by the shRNAs, were expressed. Restoring expression of DLC1 efficiently rescued endothelial sprouting capacity (Fig. 4C). Western blot analysis confirmed the knockdown and expression of the GFP-tagged DLC1 (Fig. 4D). Overall, the data indicate that endothelial DLC1 expression levels tightly control sprouting angiogenesis.

DLC1 rescues the migration and sprouting defects in YAP-depleted endothelial cells

Endothelial YAP/TAZ activation drives angiogenesis by controlling endothelial collective migration and vessel remodeling (Neto et al., 2018; Kim et al., 2017). The transcriptional targets of YAP/TAZ that are responsible for this task remain unknown. Since DLC1 is needed for collective migration and angiogenic sprouting, we next assessed the contribution of DLC1 as downstream target of YAP.

First, YAP expression was silenced using shRNAs. The knockdown of YAP in HUVECs, which is accompanied by a downregulation of DLC1 expression, inhibited scratch wound migration (Figs 5A–C and 1E), confirming previous findings (Neto et al., 2018). Immunofluorescence imaging further revealed that the defective scratch wound migration of YAP-depleted HUVECs is accompanied by the formation of perpendicularly oriented focal adhesions and actin stress fibers in cells at the leading edge (Fig. 5D), reminiscent of the morphology of DLC1-depleted HUVECs in scratch wound assays. To investigate the contribution of DLC1 as target of YAP in focal adhesion remodeling during collective migration, DLC1 protein levels were restored in shYAP HUVECs by ectopic expression of GFP–DLC1 (Fig. 5C). Ectopic expression of DLC1 in shYAP HUVECs, induced proper alignment of focal adhesions and the actin cytoskeleton of cells at the leading edge, and partially rescued the collective cell migration defects of YAP-depleted cells (Fig. 5A–D). Next, to address the contribution of DLC1 in YAP-dependent sprouting angiogenesis, the cells were analyzed for their sprouting capacity. Intriguingly, restoring DLC1 levels by ectopic expression of DLC1 fully rescued the sprouting defects of YAP-depleted HUVECs (Fig. 5E). Taken together, these findings point towards a crucial and prominent role for DLC1 in YAP/TAZ-driven endothelial adhesion remodeling and collective migration during angiogenesis.

DISCUSSION

The nuclear translocation of YAP/TAZ during stiffness and flow sensing tightly controls cell–ECM interactions, yet the downstream targets of YAP/TAZ that are responsible for such mechanoresponses still remain unclear (Totaro et al., 2018). Our study reveals that the focal adhesion protein DLC1 is a direct transcriptional target of YAP/TAZ and TEAD, and is crucial for YAP-driven collective cell migration and sprouting angiogenesis by endothelial cells. These findings implicate DLC1 in related YAP/TAZ-driven mechanotransduction processes, such as flow sensing, contact inhibition and the development of stiffness-related vascular disease.

DLC1 and the regulation of endothelial adhesion dynamics

YAP/TAZ are important mechanotransducers that translocate to the nucleus upon cell–ECM adhesion-induced actomyosin tension (Dupont et al., 2011). In turn, YAP/TAZ activation has been shown to control focal adhesions in various cell types (Nardone et al., 2017). Endothelial focal adhesions have recently been shown to provide feedback signals to YAP/TAZ activity to limit adhesion maturation for cell orientation and persistent migration (Mason et al., 2019). Intriguingly, our data now demonstrate that DLC1, following activation of YAP/TAZ, restricts focal adhesion lifetime, confines integrin-based traction forces and thereby promotes cell polarization during directed migration. These findings suggest that upregulation of DLC1 expression upon YAP/TAZ activation provides the feedback signals for optimal adhesion remodeling and force transduction.

It is still uncertain how DLC1 controls the turnover of focal adhesions and endothelial dynamics. Adhesion turnover is steered by spatiotemporal activation of Rho GTPases and subsequent cytoskeletal remodeling (Webb et al., 2002; Etienne-Manneville and Hall, 2002). DLC1 is widely known as a Rho GAP protein that acts to inhibit GTP-loading of Rho GTPases (Wong et al., 2003; Healy et al., 2008). The GAP activity of DLC1 contributes to the tumor-suppressive functions of DLC1 (Healy et al., 2008; Ko et al., 2013). However, we find no major differences in RhoA activation upon depletion of DLC1, pointing towards an alternative function of DLC1 in endothelial adhesion remodeling. In epithelial cells DLC1

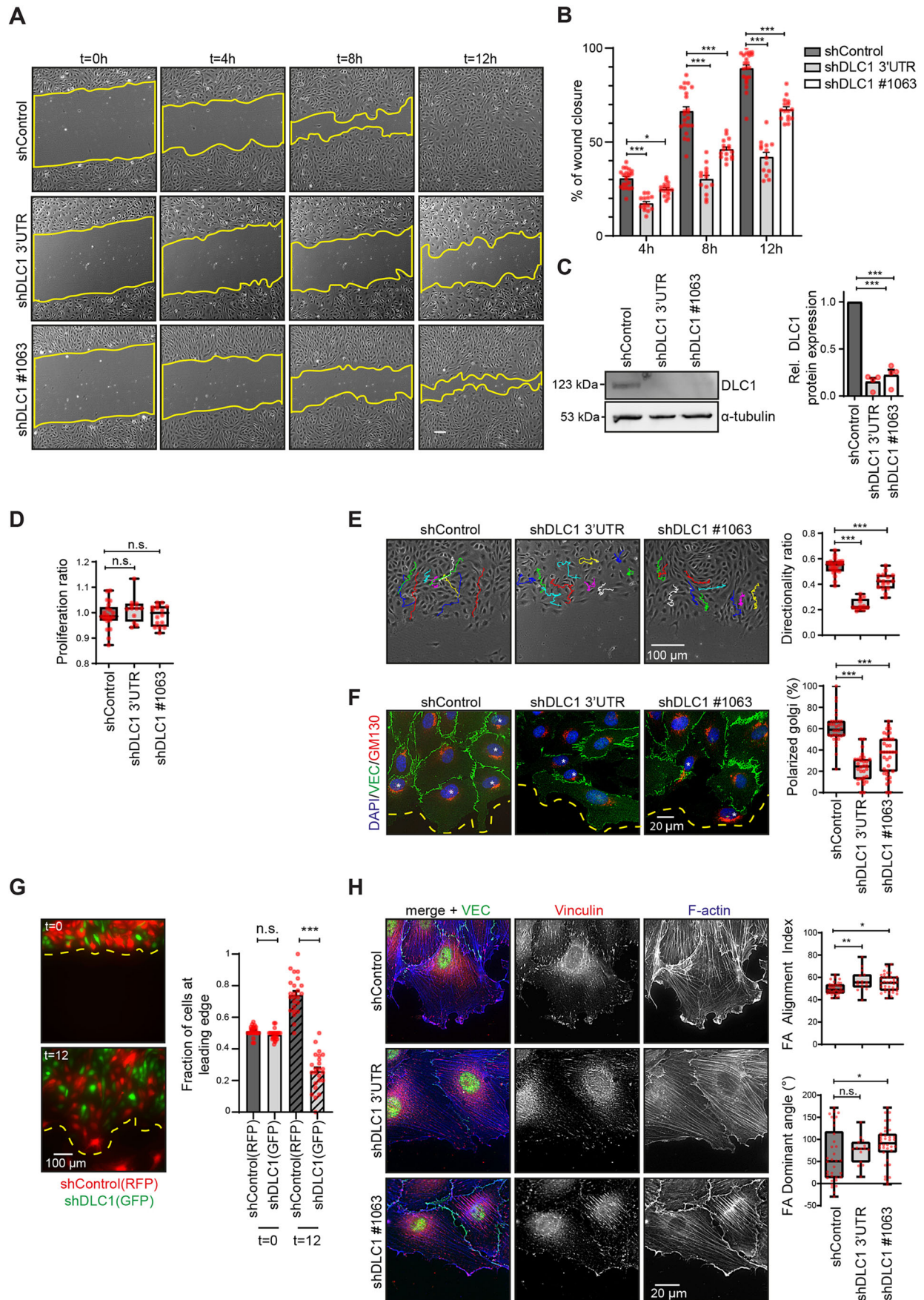


Fig. 3. See next page for legend.

Fig. 3. DLC1 is required for cell orientation and directional migration.

(A) Representative phase-contrast images of HUVECs transduced with shControl, shDLC1 3'UTR or shDLC1 #1063, in a scratch-wound assay ($t=0$, $t=4$, $t=8$ and $t=12$ h after scratch). The yellow lines highlight the unclosed wound area. See corresponding Movie 2 for the ~16 h time-lapse recording. (B) Graph showing the mean \pm s.e.m. percentage of wound closure of HUVECs transduced with shControl, shDLC1 3'UTR or shDLC1 #1063 at three time points during scratch-wound assay. Data are from four independent experiments; shControl (22 movies), shDLC1 3'UTR (14 movies) and shDLC1 #1063 (18 movies). * $P<0.05$, *** $P<0.001$ (two-way ANOVA and Tukey's multiple comparison test). (C) Representative western blot analysis of DLC1 and α -tubulin (loading control) in total lysates of HUVECs transduced with shControl, shDLC1 3'UTR or shDLC1 #1063. Graph shows mean \pm s.e.m. DLC1 protein expression level signal corrected for background and normalized to expression in shControl-transduced HUVECs. Data from four independent experiments. *** $P<0.001$ (paired Student's t -test). Scans of whole western blots are depicted in Fig. S4. (D) Box-plot showing the median (and upper and lower quartiles) for the proliferation ratio of the shControl, shDLC1 3'UTR, shDLC1 #1063 HUVECs corresponding to the scratch assays in B. The proliferation ratio was manually determined by counting cell numbers at regions of interest (ROIs) within the endothelial monolayers before and after 12 h scratch wound migration. n.s., not significant (one-way ANOVA with Dunnett's multiple comparison test). (E) Phase-contrast images of scratch wound assays overlaid with single-cell tracking analysis for 8 h as determined using the Chemotaxis Tool in ImageJ. Box-plot showing the median (and upper and lower quartiles) velocity and directionality of shControl, shDLC1 3'UTR or shDLC1 #1063-transduced HUVECs. Whiskers show the range. Data are from four independent experiments; shControl (429 cells from 22 movies), shDLC1 3'UTR (236 cells from 12 movies), shDLC1 #1063 (303 cells from 18 movies) *** $P<0.001$ (one-way ANOVA and Dunnett's multiple comparison test). (F) Widefield immunofluorescence images of HUVECs transduced with shControl, shDLC1 3'UTR or shDLC1 #1063 6 h after initiation of scratch wound assays stained for DAPI (blue), GM130 (red; Golgi) and VE-cadherin (green). Cells were considered polarized if the Golgi was located within an angle between 60° and -60° towards the migration front. The yellow dashed lines indicate the migration front and the asterisks indicate cells containing an oriented Golgi in the direction of scratch wound migration. Box-plot showing the median (and upper and lower quartiles) of cells with an oriented Golgi. Data are from three independent experiments; shControl (34 images), shDLC1 3'UTR (30 images), shDLC1 #1063 (35 images). *** $P<0.001$ (one-way ANOVA with Dunnett's multiple comparison test). (G) Representative fluorescence images of HUVECs transduced with shControl-RFP or shDLC1 3'UTR and subsequently with GFP in a scratch wound assay ($t=0$ and $t=12$ h after scratch). The yellow dashed line highlights the migration front. Graph shows the proportion of shControl RFP or shDLC1 GFP cells at the leading edge at $t=0$ and $t=12$ h after scratch. Data are from three independent experiments; shControl RFP (24 movies), shDLC1 3'UTR GFP (24 movies). *** $P<0.001$; n.s., not significant (one-way ANOVA with Dunnett's multiple comparisons test). (H) Widefield immunofluorescence images of HUVECs transduced with shControl, shDLC1 3'UTR or shDLC1 #1063 6 h after initiation of scratch wound assays stained for vinculin (red), F-actin (blue) and VE-cadherin (green). Boxplots show the median (and upper and lower quartiles) focal adhesion alignment index and focal adhesion dominant angle as determined by image analysis of the vinculin channels using the focal adhesion analysis server (Berginski and Gomez, 2013). Whiskers show the range. Data are from three independent experiments; shControl (34 images), shDLC1 3'UTR (15 images), shDLC1 #1063 (36 images). * $P<0.05$, ** $P<0.01$; n.s., not significant (one-way ANOVA with Dunnett's multiple comparison test).

is involved in migration through a GAP-independent mechanism (Shih et al., 2012), and in HeLa cells the recruitment of DLC1 to focal adhesions is needed for its pro-migratory function (Kawai et al., 2009). DLC1 has been shown to interact with the integrin-related talin and tensin proteins, as well as focal adhesion kinase (FAK, also known as PTK2) (Qian et al., 2007; Liao and Lo, 2008; Li et al., 2011; Zacharchenko et al., 2016). Interestingly, tension-induced conformational unfolding of talin, a key mechanosensor for integrins, inhibits its interaction with DLC1 and prevents downstream inhibition of myosin phosphorylation

(Haining et al., 2018). Thus, interaction between DLC1 and talin proteins might regulate myosin-driven turnover of focal adhesions to favor migration. The finding that focal adhesions align more in the absence of DLC1 during collective migration correlates with the observation that DLC1 knockdown resulted in the formation of prominent aligned basal F-actin fibers that terminate at the focal adhesions (Figs 2B and 3H). The increased focal adhesion alignment fits with the concept that the presence of basal F-actin stress fibers is indicative of focal adhesion maturation and force transmission to the ECM (Soiné et al., 2015), which is supported by the observations that a longer lifetime of the focal adhesions and increased traction forces were detected in DLC1-depleted cells (Fig. 2H,I).

Of note, in fibroblasts and various cancer cell types, DLC1 seems to have an opposing role in cell migration (Heering et al., 2009; Barras and Widmann, 2014; Kaushik et al., 2014), which might relate to differences in YAP/TAZ mechanosensing and indicates that the function of DLC1 is highly dependent on the cellular microenvironment. Within blood vessels, mechanotransduction through integrins predominantly occurs in arterial endothelium (Van Geemen et al., 2014; Di Russo et al., 2017), suggesting that the regulation of focal adhesions by DLC1 could be of particular importance in arteries.

The role of YAP/TAZ and DLC1 in angiogenesis

YAP/TAZ signaling serves prominent roles in vascular biology and angiogenesis (Choi et al., 2015; Nakajima et al., 2017; Wang et al., 2016a, 2017; Neto et al., 2018). YAP/TAZ is regulated by ECM rigidity, (blood) flow and cell density, mechanical cues that also influence angiogenesis (Zhao et al., 2007; Aragona et al., 2013; Wang et al., 2016a,b; Boerckel et al., 2011). In addition, the angiogenesis process is supported by mechanical stretch- and VEGF-mediated activation of YAP/TAZ (Neto et al., 2018; Wang et al., 2017). Our experiments using YAP-5SA show that constitutive YAP activation is sufficient to drive DLC1 expression irrespective of the stiffness of the substrate. The data suggest that constitutive activation of YAP overrules the substrate-mediated regulation of DLC1 expression. Interestingly, microarray analysis of HUVECs expressing constitutive nuclear YAP and TAZ mutants, which induce hypersprouting in angiogenesis, also revealed that there was an upregulation of DLC1 expression among the regulation of other transcriptional programs (Neto et al., 2018). We now reveal that DLC1 is needed for VEGF-induced sprouting, and that ectopic DLC1 expression is sufficient to restore migration and sprouting in YAP-depleted endothelial cells. Of note, previous studies have demonstrated that TAZ serves an even stronger role during collective migration (Neto et al., 2018). Whether DLC1 is also capable of restoring collective migration during sprouting in TAZ-deficient endothelial cells remains to be examined in future studies. DLC1 and the related protein DLC2 (also known as STARD13) have been shown to contribute to experimentally induced angiogenesis *in vivo* (Shih et al., 2017; Lin et al., 2010). Moreover, DLC1 was described to regulate contact inhibition of growth in endothelial cells (Sánchez-Martín et al., 2018). This fits with a model in which DLC1 expression levels are tightly controlled for endothelial rearrangements during angiogenesis. The adherens junction receptor VE-cadherin, an endothelial-specific cadherin that safeguards vascular integrity and steers endothelial dynamics (Carmeliet et al., 1999; Bentley et al., 2014), sequesters YAP at stabilized endothelial cell-cell junctions to prevent its activation (Giampietro et al., 2015). Possibly, the inhibition of YAP/TAZ nuclear translocation by VE-cadherin contributes to stabilization of

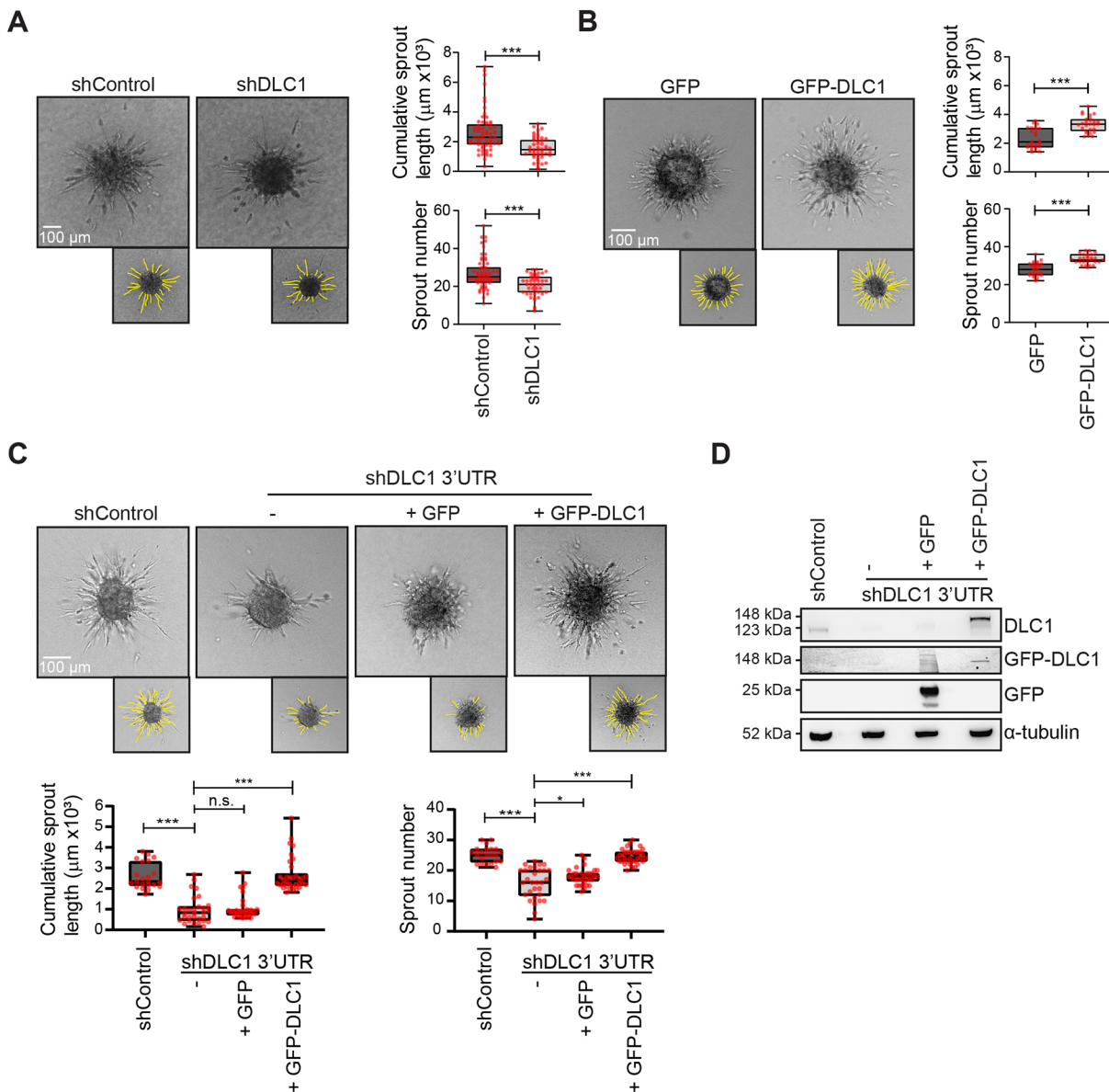


Fig. 4. DLC1 controls sprouting angiogenesis. (A) Representative phase-contrast images of sprouting spheroids 16 h after VEGF stimulation of HUVECs lentivirally transduced with shControl or shDLC1 (pool of #1063 and #1064). Box-plot shows the median (and upper and lower quartiles) cumulative sprout length and the number of sprouts in the spheroid-based sprouting angiogenesis assays. Whiskers show the range. Data are from three independent experiments; shControl (63 spheroids), shDLC1 (47 spheroids). $***P < 0.001$ (two-tailed unpaired Student's *t*-test). (B) Representative phase-contrast images of sprouting spheroids 16 h after VEGF stimulation of HUVECs lentivirally transduced with GFP or GFP-DLC1. Box-plot shows the median (and upper and lower quartiles) cumulative sprout length and the number of sprouts in the spheroid-based sprouting angiogenesis assays. Whiskers show the range. Data are from three independent experiments; GFP (25 spheroids), GFP-DLC1 (27 spheroids). $***P < 0.001$ (two-tailed unpaired Student's *t*-test). (C) Representative phase-contrast images of sprouting spheroids 16 h after VEGF stimulation of HUVECs transduced with shControl or shDLC1 3'UTR and rescued with GFP or GFP-DLC1. Box-plots show the median (and upper and lower quartiles) cumulative sprout length and number of sprouts per spheroid. Whiskers show the range. Data are from three independent experiments, shControl (33 spheroids), shDLC1 3'UTR (29 spheroids), rescue GFP (39 spheroids), rescue GFP-DLC1 (37 spheroids). n.s., not significant; $*P < 0.05$; $***P < 0.001$ (one-way ANOVA with Dunnett's multiple comparisons test). In A–C, smaller images underneath main phase-contrast images show the overlaid quantified sprouts in yellow. (D) Representative western blot analysis of DLC1, GFP and α -tubulin (loading control) in lysates of HUVECs transduced with shControl or shDLC1 3'UTR and rescued with GFP or GFP-DLC1. Note that the GFP-tagged DLC1 has a higher molecular mass than endogenous DLC1. Scans of whole western blots are depicted in Fig. S4.

blood vessel integrity through suppression of DLC1-driven endothelial migration and/or angiogenic sprouting.

Disturbed crosstalk between DLC1 and YAP/TAZ in pathology?

DLC1 expression is elevated in the endothelium of atherosclerotic plaques and in pulmonary hypertension (Schimmel et al., 2018).

The development of these cardiovascular diseases is driven by pathological stiffening and disturbed flow patterns (Huvencers et al., 2015), which activate endothelial YAP/TAZ (Wang et al., 2016a,b; Bertero et al., 2016). Therefore, targeting of YAP/TAZ, or their downstream targets such as DLC1, holds promise as therapeutic approach in stiffness-related vascular diseases. Of interest, mutations in the YAP and TAZ genes (Antonescu, 2014)

Fig. 5. DLC1 rescues the migration and sprouting defects in YAP-depleted endothelial cells. (A) Phase-contrast images of HUVECs transduced with shControl or shYAP and rescued with GFP or GFP–DLC1, in a scratch-wound assay ($t=0$, $t=4$, $t=8$ and $t=12$ h after scratch). The yellow line highlights the unclosed wound area. (B) Graph showing the mean \pm s.e.m. percentage of wound closure of HUVECs transduced with shControl or shYAP and rescued with GFP or GFP–DLC1 at three time-points during the scratch-wound assay. Data are from three independent experiments; shControl (14 movies), shYAP (14 movies), rescue GFP (11 movies), rescue GFP–DLC1 (7 movies). * $P<0.05$; *** $P<0.001$; n.s., not significant (one-way ANOVA with Dunnett's multiple comparisons test). (C) Western blot analysis of DLC1, YAP, GFP and β -actin in lysates of HUVECs transduced with shControl, shYAP and rescued with GFP or GFP–DLC1. Scans of whole western blots are depicted in Fig. S4. (D) Representative widefield IF images of HUVECs transduced with shControl or shYAP, or shYAP-transduced HUVECs expressing GFP or GFP–DLC1, 6 h after initiation of scratch wound assay. Stained for Vinculin (red) and F-actin (green). The asterisks indicate the GFP-positive cells (not shown). (E) Representative phase-contrast images of sprouting spheroids 16 h after VEGF stimulation of HUVECs transduced with shControl, shYAP and rescued with GFP or GFP–DLC1. Smaller images underneath main phase-contrast images show the overlaid quantified sprouts in yellow. Box-plots show the median (and upper and lower quartiles) cumulative sprout length and number of sprouts per spheroid. Whiskers show the range. Data are from three independent experiments; shControl (27 spheroids), shYAP (18 spheroids), rescue GFP (21 spheroids), rescue GFP–DLC1 (28 spheroids). * $P<0.05$, *** $P<0.001$; n.s., not significant (one-way ANOVA with Dunnett's multiple comparison test).

(Ritchey et al., 2019). This would fit with a model in which YAP/TAZ and DLC1 control each other via feedback mechanisms that are sensed at focal adhesions. Because DLC1 is expressed in many cell types beyond the endothelium, and because DLC1 has been identified as a tumor suppressor in various types of cancer (Liao and Lo, 2008; Durkin et al., 2007), we postulate that DLC1 might also function in YAP/TAZ-driven cancer cell behavior, and other epithelial tissue processes that involve remodeling of integrin-based adhesions.

MATERIALS AND METHODS

Antibodies and reagents

Purified mouse anti-human DLC1 [Clone 3, Cat# 612021, diluted 1:1000 for western blotting (WB)] and purified mouse anti-GM130 [clone 35, Cat# 610823, diluted 1:200 for immunofluorescence (IF)] were obtained from BD Biosciences. To visualize VE-cadherin we used purified mouse anti-cadherin-5 (BD Biosciences, clone 75, Cat# 610252, diluted 1:100 for IF) and rabbit polyclonal anti-VE-cadherin (Cayman Chemical, Cat # 160840, diluted 1:100 for IF). Rabbit polyclonal anti-phospho-paxillin (Tyr118) (Cat# 44-722G, diluted 1:200 for IF) was from Thermo Fischer Scientific. Mouse monoclonal anti-vinculin (hVIN-1 clone, Cat# V9131, diluted 1:400 for IF) and rabbit polyclonal anti-WWTR1 (anti-TAZ, Cat# HPA007415, diluted 1:1000 for WB) were obtained from Sigma-Aldrich. We used rabbit polyclonal anti-YAP1 (Genetex, Cat# GTX129151, diluted 1:1000 for WB) to detect YAP, mouse monoclonal anti-c-Myc (clone 9E10, Cat# SC-40, diluted 1:1000 for WB) and goat polyclonal anti CTGF (Santa Cruz Biotechnology, L-20, Cat # sc-14939, diluted 1:1000 for WB) to detect CTGF. To detect GFP we used the monoclonal mouse anti-GFP antibody (Santa Cruz Biotechnology, B-2, Cat # sc-9996, 1:1000 for WB). As a loading control, we stained with mouse monoclonal anti-human α -tubulin (Cedarlane, Clone DM1A, Cat# CLT9002, diluted 1:10,000 for WB) or rabbit polyclonal anti- β -actin (Cell Signaling, Cat# 4967S, diluted 1:1000 for WB). Secondary antibodies coupled to Alexa Fluor 488, 594 and 647, were purchased from Invitrogen (diluted 1:100 for IF). To visualize F-actin we used PromoFluor-415-phalloidin (Promokine, Cat# PK-PF415-7-01, diluted 1:200 for IF), Alexa Fluor 568-phalloidin (Thermo Fisher Scientific, Cat# A12380, diluted 1:200 for IF) or Texas Red-X Phalloidin (Thermo Fisher, Cat# T7471, diluted 1:200 for IF). DAPI was used for nuclear immunofluorescence stainings (Invitrogen, diluted 1:1000). Secondary antibodies coupled to horseradish peroxidase (HRP) were obtained from Bio-Rad (diluted 1:1000 for WB). Thrombin (used at

0.2 U/ml) was from Haematologic Technologies. Doxycyclin (used at 1 ng/ml) was from Sigma-Aldrich.

Cell culture

Pooled primary HUVECs (cultured up to passage six) from different donors (Lonza) were cultured in Endothelial Cell Growth Medium 2 culture medium supplemented with the Growth Medium 2 Supplement Pack (PromoCell) on gelatin-coated tissue flasks. 2 kPa or 50 kPa hydrogels (Matrigen) were activated with PBS and coated with $5 \mu\text{g ml}^{-1}$ fibronectin overnight. HEK293T cells (ATCC) were cultured in Dulbecco's modified Eagle's medium with L-glutamine supplemented with 10% fetal bovine serum and antibiotics. Cells were recently authenticated and tested for contamination.

DNA plasmids and lentiviral transductions

shRNAs in the lentiviral pLKO.1 backbone targeting DLC1 (TRCN47823, 47824, 47825, 47826 and 47827, which in this manuscript are referred to as plasmid numbers #1063, #1064, #1065, #1066 and #1067 respectively), YAP1 (TRCN107265), TAZ (TRCN19473) and control shRNA (shC002) with or without tagRFP were from Sigma-Aldrich mission library. A modified version of the pLKO.1 plasmid was generated based on the 5'-GGAGTGATAGGAATTGACTATA-3' sequence to express shRNA that target the 3'-UTR of human DLC1 mRNA. Full-length human DLC1 fused at its N-terminus to a GFP tag was amplified by PCR from a pEGFP-C1-DLC1 vector (provided by Xiaolan Qian and Douglas Lowy, NIH, Bethesda, MD) and cloned into a self-inactivating lentiviral pLV-CMV-ires-puro vector between the SnaBI and XbaI restriction sites. For the pInducer20-myc-hYAP1-5SA-Ubc construct, human YAP1 with S61A, S109A, S127A, S164A, S381A mutations was amplified by PCR from a pQCXIIH vector (Zhao et al., 2007) and through Gateway Recombination cloned into a pInducer20 vector with Ubc promoter (Meerbrey et al., 2011). The pRRL paxillin-mCherry construct was a gift from Olivier Pertz (University of Basel, Switzerland) and pLenti-GFP from Johan de Rooij (UMC Utrecht, The Netherlands). Luciferase reporter constructs are based on a pGL3 basic luciferase reporter vector (Promega), containing a firefly luciferase gene. The DLC1 promoter region (–418 to +319 bp from the transcriptional start site) containing the wild-type TEAD motif (CATTCCA) or a mutated motif (AGACTAT) were purchased from GenScript and inserted at the 5' end of the luciferase gene between NheI and BglIII restriction sites. To produce lentiviral particles, HEK293T cells were transfected with third-generation packaging constructs and lentiviral expression vectors using Trans-IT-LTI transfection reagents (Mirus). Lentivirus containing supernatant was harvested 48–72 h post transfection. HUVECs, cultured up to ~80% confluency, were transduced with lentiviral particles overnight. shRNA-based knockdown cells were analyzed at least 48 h after transduction. For TIRF microscopy, HUVECs were first transduced with shDLC1 or shControl lentivirus, and subsequently transduced with paxillin-mCherry lentivirus. Expression of YAP-5SA was induced by doxycyclin treatment for 48 h.

Electric cell-substrate impedance sensing

ECIS was used to analyze endothelial barrier function. Electrode arrays (8W10E; IBIDI) were treated with 10 mM L-cysteine (Sigma-Aldrich) for 15 min at 37°C. After washing with 0.9% NaCl, the arrays were coated with $10 \mu\text{g ml}^{-1}$ fibronectin in 0.9% NaCl for 1 h at 37°C. Cells were seeded on the arrays and the impedance was measured during monolayer formation at 4 kHz using the ECIS model ZTheta (Applied BioPhysics).

G-LISA – RhoA activity assays

For analysis of RhoA activity, confluent HUVECs were washed with ice-cold PBS and lysed in lysis buffer from the RhoA G-LISA activation kit (Cytoskeleton). RhoA activity was determined according to manufacturer's protocol.

Immunofluorescence stainings

For standard immunofluorescence stainings, cells were cultured on coverslips coated with $5 \mu\text{g ml}^{-1}$ fibronectin. Cells were fixed by 10 min

incubation with 4% paraformaldehyde in PBS⁺⁺ (PBS with 1 mM CaCl₂ and 0.5 mM MgCl₂). Fixed cells were permeabilized for 5 min with 0.5% Triton X-100 in PBS and blocked for 30 min in 2% BSA in PBS. Primary and secondary antibodies were diluted in 0.5% BSA in PBS and incubated for 45 min. After each step, the fixed cells were washed three times with 0.5% BSA in PBS. Coverslips were mounted in Mowiol4-88/DABCO solution.

Luciferase assays

HEK293 cells were seeded sparsely (75,000 cells per well) in 24-well plates coated with gelatin. Cells were transfected with the pGL3-DLC1-promoter luciferase reporter plasmids using PEI (Polysciences). pRL-TK Renilla reporter plasmid was co-transfected (1:50) as a control for transfection efficiency. At 2 days after transfection firefly and *Renilla* luciferase activities were analyzed using the Dual-Luciferase Reporter Assay System (Promega) and the GloMax-Multi detection system (Promega) according to manufacturer's protocol.

Quantitative PCR

Total RNA was isolated from HUVECs using TRI Reagent (Sigma). cDNA synthesis was performed using iScript (Bio-Rad). Quantitative polymerase chain reaction was performed using SensiFAST SYBR Green No-ROX (Bioline) on a LightCycler 480 system (Roche). To calculate the relative gene expression, the $\Delta\Delta C_t$ method was used. DLC1 expression was corrected for RPLP0 reference expression, and DLC1 expression levels were normalized to its levels on plastic. Primer sequences were as follows: DLC1 forward 5'-ATGATCGCCGAGTGCAAGAA-3' and reverse 5'-CTGCTCCGAAGTGGAGTAGC-3'. RPLP0 forward 5'-TCGACAATGGCAGC-ATCTAC-3' and reverse 5'-ATCCGTCTCCACAGACAAGG-3'.

Scratch assays

For scratch assays, HUVECs were plated on 12-well or 24-well plates coated with 5 $\mu\text{g ml}^{-1}$ fibronectin. Two perpendicular scratches per well were made using a sterile 200 μl pipette tip. Next, cells were washed with PBS⁺⁺, cultured in EGM-2 medium, and were mounted on an inverted NIKON Eclipse TI microscope equipped with an Okolab cage incubator and humidified CO₂ gas chamber set to 37°C and 5% CO₂. Cells were live imaged (for 16–20 h; 10 min time interval) using phase-contrast imaging using a 10 \times CFI Achromat DL dry objective (NA 0.25) and an Andor Zyla 4.2 plus sCMOS camera. Images were enhanced for display with an unsharp mask filter and adjusted for brightness and contrast in ImageJ. Scratch wounding surface was quantified by measuring the wound area using the freehand tool in ImageJ. The ImageJ manual tracking plugin was used for single-cell tracking, and the Chemotaxis tool was used to quantify directionality and velocity. For immunofluorescence stainings of scratch assays, cells were plated on coverslips coated with 5 $\mu\text{g ml}^{-1}$ fibronectin and fixed after 6 h with 4% PFA. Golgi orientation was assessed by measuring the center of mass of the DAPI and GM130 signal and calculating the angle between these points in relation to the direction of migration. Focal adhesion orientation was analyzed using the focal adhesion server using a minimal adhesion size of 4 pixels and a maximal adhesion size of 115 pixels (Berginski and Gomez, 2013).

Sprouting angiogenesis assays

For sprouting angiogenesis assays, HUVECs were resuspended in EGM-2 medium containing 0.1% methylcellulose (4000 cP, Sigma). For spheroid formation, 750 cells per 100 μl methylcellulose medium were seeded in wells of a U-bottom 96-wells plate and incubated overnight. Spheroids were collected and resuspended in 1.7 mg/ml collagen type I rat tail mixture (IBIDI), plated in glass-bottom 96-well plates and placed at 37°C. After polymerization of the collagen gel, spheroids were stimulated with 50 ng ml⁻¹ VEGF to induce sprouting overnight as described previously (Korff and Augustin, 1999). Pictures were taken using the EVOS M7000 imaging system and a 10 \times objective. Images were enhanced for display with an unsharp mask filter and adjusted for brightness and contrast in ImageJ. Sprouting number and length was analyzed using the ImageJ plugin NeuronJ.

Fluorescence microscopy

For live-cell fluorescence microscopy, cells were plated on Lab-Tek chambered 1.0 borosilicated coverglass slides coated with 5 $\mu\text{g ml}^{-1}$ fibronectin and cultured in EGM2 culture medium. For TIRF microscopy, we used an inverted NIKON Eclipse TI equipped with a 60 \times 1.49 NA Apo TIRF (oil) objective, perfect focus system, Orange Diode Solid State Laser 594 nm 30 mW (Excelsior, Spectra-physics), dual band 488/594 nm TIRF filter cube (Chroma TRF59905 ET), and an Andor Zyla 4.2 plus sCMOS camera (without binning). An Okolab cage incubator and humidified CO₂ gas chamber set to 37°C and 5% CO₂ were used during the imaging process. Image acquisition was performed every 30 s interval for 3–5 h. To analyze focal adhesion dynamics, the raw data was uploaded to the focal adhesion server using a minimal adhesion size of 4 pixels and phase length of 5 min (Berginski and Gomez, 2013). For widefield microscopy of immunostained HUVECs, the NIKON Eclipse TI was equipped with a lumencor SOLA SE II light source and standard DAPI, GFP, mCherry or Cy5 filter cubes (NIKON). Samples stained for immunofluorescence in Fig. 2B,F were imaged using an inverted Zeiss widefield microscopes Observer.Z1 equipped with a 63 \times 1.40 Plan Apochromat oil objective and a Hamamatsu Orca-R2 digital camera. Images were enhanced for display with an unsharp mask filter and adjusted for brightness and contrast in ImageJ.

Traction force microscopy

For traction force microscopy, HUVECS were plated on collagen-coated 1.2 kPa (Young's modulus) polyacrylamide substrates containing 2 μm reference bottom beads and 0.2 μm sulfated top beads (FluoSpheres, Molecular Probes). HUVECS were cultured to confluency on the gels for 48 h, and subsequently visualized using an inverted Zeiss Axiovert 200 widefield microscope equipped with a 40 \times 0.75 NA Zeiss air objective, Cooke Sensicam CCD camera and IBIDI climate-control system. To determine traction forces, the top and reference beads were imaged using fluorescence microscopy and DIC to visualize the HUVECs. Finally, the HUVECs were trypsinized from the substrate to acquire images of the unloaded fiducial bead patterns. Computation of traction forces was performed as described previously using known material properties (stiffness=1.2 kPa, Poisson's ratio=0.48) and the constrained two-dimensional fast Fourier transformation method (Valent et al., 2016). From the monolayer traction fields, the root mean squared value of traction in pascals was calculated as scalar measure for monolayer traction.

Western blot analysis

Cells were lysed with reduced sample buffer containing 4% β -mercaptoethanol. Samples were boiled at 95° for 5–10 min to denature the proteins. 10% SDS-PAGE gels were used in SDS-page running buffer (25 mM Tris-HCl pH 8.3, 192 mM glycine and 0.1% SDS), and transferred to ethanol-activated PVDF membrane using wet transfer in blot buffer [25 mM Tris-HCl pH 8.3, 192 mM glycine and 20% (v/v) ethanol]. Blots were blocked with 5% milk powder or BSA in Tris-buffered saline (TBS) for 30 min. Blots were incubated overnight at 4°C with the primary antibodies in 5% milk/BSA in TBS with Tween-20 (TBST). The secondary antibodies linked to horseradish peroxidase (HRP) were incubated with the membrane for 45 min at room temperature. As final step before imaging, blots were washed with TBS. HRP signals were visualized by enhanced chemiluminescence (ECL) detection (SuperSignal West Pico PLUS, Thermo Fisher, Cat # 34580) and visualized with a ImageQuant LAS 4000 (GE Healthcare) machine. Intensities of bands were quantified by using the Gel Analyzer plugin in ImageJ.

Acknowledgements

We are grateful to Dr Peter Stroeken (Amsterdam UMC, University of Amsterdam, the Netherlands) for providing lentiviral shRNAs from the MISSION library (Sigma-Aldrich) of the RNAi Consortium, Mirjam van der Net (University Medical Center Utrecht, the Netherlands) for cloning the YAP-5SA plasmid, and Dr Koen Prange for assistance with TEAD motif screens. Dr Holger Gerhardt (Max-Delbrück Center for Molecular Medicine, Berlin, Germany), Dr Noam Zelcer (Amsterdam UMC, University of Amsterdam, the Netherlands), Dr Nathalie Reinhard (Amsterdam UMC, University of Amsterdam, the Netherlands) and Dr Johan de Rooij (University Medical Center Utrecht, the Netherlands) are thanked for insightful scientific discussions.

Competing interests

The authors declare no competing or financial interests.

Author contributions

Conceptualization: M.v.d.S., L.S., M.G., J.D.v.B., S.H.; Methodology: A.-M.v.S., E.T.V., S.H.; Validation: M.v.d.S., K.N., A.-M.v.S., A.d.H., E.T.V., D.S.K., J.D.v.B., S.H.; Formal analysis: M.v.d.S., L.S., K.N., A.-M.v.S., A.d.H., A.K.-B., E.T.V., D.S.K., G.P.v.N.A., V.d.W., M.G., J.D.v.B., S.H.; Investigation: M.v.d.S., L.S., K.N., A.-M.v.S., A.d.H., A.K.-B., E.T.V., G.P.v.N.A., V.d.W., M.G., J.D.v.B., S.H.; Resources: M.G.; Writing - original draft: M.v.d.S., S.H.; Writing - review & editing: M.v.d.S., C.J.d.V., V.d.W., M.G., J.D.v.B., S.H.; Visualization: D.S.K.; Supervision: G.P.v.N.A., C.J.d.V., V.d.W., J.D.v.B., S.H.; Project administration: S.H.; Funding acquisition: V.d.W., M.G., J.D.v.B., S.H.

Funding

This study was financially supported by the Nederlandse Organisatie voor Wetenschappelijk Onderzoek (NWO-VIDI grant 016.156.327 to S.H.; NWO-VIDI grant 016.189.166 to M.G.; NWO gravitational program CancerGenomiCs.nl to M.G.) and the Rembrandt Institute for Cardiovascular Diseases (to J.D.v.B and V.d.W.).

Supplementary information

Supplementary information available online at <http://jcs.biologists.org/lookup/doi/10.1242/jcs.239947.supplemental>

Peer review history

The peer review history is available online at <https://jcs.biologists.org/lookup/doi/10.1242/jcs.239947.reviewer-comments.pdf>

References

- Antonescu, C.** (2014). Malignant vascular tumors—an update. *Mod. Pathol.* **27**, S30. doi:10.1038/modpathol.2013.176
- Aragona, M., Panciera, T., Manfrin, A., Giullitti, S., Michielin, F., Elvassore, N., Dupont, S. and Piccolo, S.** (2013). A mechanical checkpoint controls multicellular growth through YAP/TAZ regulation by actin-processing factors. *Cell* **154**, 1047–1059. doi:10.1016/j.cell.2013.07.042
- Astone, M., Lai, J. K. H., Dupont, S., Stainier, D. Y. R., Argenton, F. and Vettori, A.** (2018). Zebrafish mutants and TEAD reporters reveal essential functions for Yap and Taz in posterior cardinal vein development. *Sci. Rep.* **8**, 10189. doi:10.1038/s41598-018-27657-x
- Barras, D. and Widmann, C.** (2014). GAP-independent functions of DLC1 in metastasis. *Cancer Metastasis Rev.* **33**, 87–100. doi:10.1007/s10555-013-9458-0
- Bentley, K., Franco, C. A., Philippides, A., Bianco, R., Dierkes, M., Gebala, V., Stanchi, F., Jones, M., Aspalter, I. M., Cagna, G. et al.** (2014). The role of differential VE-cadherin dynamics in cell rearrangement during angiogenesis. *Nat. Cell Biol.* **16**, 309. doi:10.1038/ncb2926
- Berginski, M. E. and Gomez, S. M.** (2013). The focal adhesion analysis server: a web tool for analyzing focal adhesion dynamics. *F1000 Res.* **2**, 68. doi:10.12688/f1000research.2-68.v1
- Bertero, T., Oldham, W. M., Cottrill, K. A., Pisano, S., Vanderpool, R. R., Yu, Q., Zhao, J., Tai, Y., Tang, Y., Zhang, Y.-Y. et al.** (2016). Vascular stiffness mechanoregulates YAP/TAZ-dependent glutaminolysis to drive pulmonary hypertension. *J. Clin. Invest.* **126**, 3313–3335. doi:10.1172/JCI86387
- Betz, C., Lenard, A., Belting, H.-G. and Affolter, M.** (2016). Cell behaviors and dynamics during angiogenesis. *Development* **143**, 2249–2260. doi:10.1242/dev.135616
- Bisel, B., Calamai, M., Vanzi, F. and Pavone, F. S.** (2013). Decoupling polarization of the Golgi Apparatus and GM1 in the plasma membrane. *PLoS ONE* **8**, e80446. doi:10.1371/journal.pone.0080446
- Boerckel, J. D., Uhrig, B. A., Willett, N. J., Huebsch, N. and Goldberg, R. E.** (2011). Mechanical regulation of vascular growth and tissue regeneration in vivo. *Proc. Natl. Acad. Sci. USA* **108**, E674–E680. doi:10.1073/pnas.1107019108
- Carmeliet, P., Lampugnani, M.-G., Moons, L., Breviaro, F., Compernelle, V., Bono, F., Balconi, G., Spagnuolo, R., Oosthuysen, B., Dewerchin, M. et al.** (1999). Targeted deficiency or cytosolic truncation of the VE-cadherin gene in mice impairs VEGF-mediated endothelial survival and angiogenesis. *Cell* **98**, 147–157. doi:10.1016/S0092-8674(00)81010-7
- Choi, H.-J., Zhang, H., Park, H., Choi, K.-S., Lee, H.-W., Agrawal, V., Kim, Y.-M. and Kwon, Y.-G.** (2015). Yes-associated protein regulates endothelial cell contact-mediated expression of angiotensin-2. *Nat. Commun.* **6**, 6943. doi:10.1038/ncomms7943
- Di Russo, J., Luik, A.-L., Yousif, L., Budny, S., Oberleithner, H., Hofschroer, V., Klingauf, J., van Bavel, E., Bakker, E. N., Hellstrand, P. et al.** (2017). Endothelial basement membrane laminin 511 is essential for shear stress response. *EMBO J.* **36**, 183–201. doi:10.15252/embj.201694756
- Dorland, Y. L. and Huvencsers, S.** (2017). Cell–cell junctional mechanotransduction in endothelial remodeling. *Cell. Mol. Life Sci.* **74**, 279–292. doi:10.1007/s00018-016-2325-8
- Dupont, S.** (2016). Role of YAP/TAZ in cell-matrix adhesion-mediated signalling and mechanotransduction. *Exp. Cell Res.* **343**, 42–53. doi:10.1016/j.yexcr.2015.10.034
- Dupont, S., Morsut, L., Aragona, M., Enzo, E., Giulitti, S., Cordenonsi, M., Zanconato, F., Le Digabel, J., Forcato, M., Bicciato, S. et al.** (2011). Role of YAP/TAZ in mechanotransduction. *Nature* **474**, 179. doi:10.1038/nature10137
- Durkin, M. E., Avner, M. R., Huh, C.-G., Yuan, B.-Z., Thorgeirsson, S. S. and Popescu, N. C.** (2005). DLC-1, a Rho GTPase-activating protein with tumor suppressor function, is essential for embryonic development. *FEBS Lett.* **579**, 1191–1196. doi:10.1016/j.febslet.2004.12.090
- Durkin, M. E., Yuan, B.-Z., Zhou, X., Zimonjic, D. B., Lowy, D. R., Thorgeirsson, S. S. and Popescu, N. C.** (2007). DLC-1: a Rho GTPase-activating protein and tumour suppressor. *J. Cell. Mol. Med.* **11**, 1185–1207. doi:10.1111/j.1582-4934.2007.00098.x
- Eilken, H. M. and Adams, R. H.** (2010). Dynamics of endothelial cell behavior in sprouting angiogenesis. *Curr. Opin. Cell Biol.* **22**, 617–625. doi:10.1016/j.ccb.2010.08.010
- Elosegui-Artola, A., Andreu, I., Beedle, A. E. M., Lezamiz, A., Uroz, M., Kosmalka, A. J., Oria, R., Kechagia, J. Z., Rico-Lastres, P., Le Roux, A.-L. et al.** (2017). Force triggers YAP nuclear entry by regulating transport across nuclear pores. *Cell* **171**, 1397–1410.e14. doi:10.1016/j.cell.2017.10.008
- Etienne-Manneville, S. and Hall, A.** (2002). Rho GTPases in cell biology. *Nature* **420**, 629. doi:10.1038/nature01148
- Fischer, R. S., Lam, P.-Y., Huttenlocher, A. and Waterman, C. M.** (2019). Filopodia and focal adhesions: an integrated system driving branching morphogenesis in neuronal pathfinding and angiogenesis. *Dev. Biol.* **451**, 86–95. doi:10.1016/j.ydbio.2018.08.015
- Franco, C. A., Jones, M. L., Bernabeu, M. O., Geudens, I., Mathivet, T., Rosa, A., Lopes, F. M., Lima, A. P., Ragab, A., Collins, R. T. et al.** (2015). Dynamic endothelial cell rearrangements drive developmental vessel regression. *PLoS Biol.* **13**, e1002125. doi:10.1371/journal.pbio.1002125
- Gardel, M. L., Schneider, I. C., Aratyn-Schaus, Y. and Waterman, C. M.** (2010). Mechanical integration of actin and adhesion dynamics in cell migration. *Annu. Rev. Cell Dev. Biol.* **26**, 315–333. doi:10.1146/annurev.cellbio.011209.122036
- Geiger, B., Bershadsky, A., Pankov, R. and Yamada, K. M.** (2001). Transmembrane crosstalk between the extracellular matrix and the cytoskeleton. *Nat. Rev. Mol. Cell Biol.* **2**, 793. doi:10.1038/35099066
- Geiger, B., Spatz, J. P. and Bershadsky, A. D.** (2009). Environmental sensing through focal adhesions. *Nat. Rev. Mol. Cell Biol.* **10**, 21. doi:10.1038/nrm2593
- Giampietro, C., Disanza, A., Bravi, L., Barrios-Rodiles, M., Corada, M., Frittoli, E., Savorani, C., Lampugnani, M. G., Boggetti, B., Niessen, C. et al.** (2015). The actin-binding protein EPS8 binds VE-cadherin and modulates YAP localization and signaling. *J. Cell Biol.* **211**, 1177–1192. doi:10.1083/jcb.201501089
- Gomez-Salinerio, J. M. and Rafii, S.** (2018). Endothelial cell adaptation in regeneration. *Science* **362**, 1116–1117. doi:10.1126/science.aar4800
- Grashoff, C., Hoffman, B. D., Brenner, M. D., Zhou, R., Parsons, M., Yang, M. T., McLean, M. A., Sligar, S. G., Chen, C. S., Ha, T. et al.** (2010). Measuring mechanical cross vinculin reveals regulation of focal adhesion dynamics. *Nature* **466**, 263. doi:10.1038/nature09198
- Ha, T., Ohnuki, H. and Tosato, G.** (2018). Novel insights into endothelial cell malignancies. *Oncotarget* **9**, 37468–37470. doi:10.18632/oncotarget.26516
- Haining, A. W. M., Rahikainen, R., Cortes, E., Lachowski, D., Rice, A., von Essen, M., Hytönen, V. P. and del Río Hernández, A.** (2018). Mechanotransduction in talin through the interaction of the R8 domain with DLC1. *PLoS Biol.* **16**, e2005599. doi:10.1371/journal.pbio.2005599
- Healy, K. D., Hodgson, L., Kim, T.-Y., Shutes, A., Maddileti, S., Juliano, R. L., Hahn, K. M., Harden, T. K., Bang, Y.-J. and Der, C. J.** (2008). DLC-1 suppresses non-small cell lung cancer growth and invasion by RhoGAP-dependent and independent mechanisms. *Mol. Carcinog.* **47**, 326–337. doi:10.1002/mc.20389
- Heering, J., Erlmann, P. and Olayioye, M. A.** (2009). Simultaneous loss of the DLC1 and PTEN tumor suppressors enhances breast cancer cell migration. *Exp. Cell Res.* **315**, 2505–2514. doi:10.1016/j.yexcr.2009.05.022
- Heiss, M., Hellström, M., Kalén, M., May, T., Weber, H., Hecker, M., Augustin, H. G. and Korff, T.** (2015). Endothelial cell spheroids as a versatile tool to study angiogenesis in vitro. *FASEB J.* **29**, 3076–3084. doi:10.1096/fj.14-267633
- Huvencsers, S., Daemen, M. J. A. P. and Hordijk, P. L.** (2015). Between Rho(k) and a hard place: the relation between vessel wall stiffness, endothelial contractility, and cardiovascular disease. *Circ. Res.* **116**, 895–908. doi:10.1161/CIRCRESAHA.116.305720
- Kaushik, S., Ravi, A., Hameed, F. M. and Low, B. C.** (2014). Concerted modulation of paxillin dynamics at focal adhesions by deleted in liver cancer-1 and focal adhesion kinase during early cell spreading. *Cytoskeleton* **71**, 677–694. doi:10.1002/cm.21201
- Kawai, K., Iwamae, Y., Yamaga, M., Kiyota, M., Ishii, H., Hirata, H., Homma, Y. and Yagisawa, H.** (2009). Focal adhesion-localization of START-GAP1/DLC1 is

- essential for cell motility and morphology. *Genes Cells* **14**, 227–241. doi:10.1111/j.1365-2443.2008.01265.x
- Kim, T. Y., Vigil, D., Der, C. J. and Juliano, R. L. (2009). Role of DLC-1, a tumor suppressor protein with RhoGAP activity, in regulation of the cytoskeleton and cell motility. *Cancer Metastasis Rev.* **28**, 77–83. doi:10.1007/s10555-008-9167-2
- Kim, J., Kim, Y. H., Kim, J., Park, D. Y., Bae, H., Lee, D.-H., Kim, K. H., Hong, S. P., Jang, S. P., Kubota, Y. et al. (2017). YAP/TAZ regulates sprouting angiogenesis and vascular barrier maturation. *J. Clin. Invest.* **127**, 3441–3461. doi:10.1172/JCI93825
- Ko, F. C. F., Chan, L.-K., Man-Fong Sze, K., Yeung, Y.-S., Yuk-Ting Tse, E., Lu, P., Yu, M.-H., Oi-Lin Ng, I. and Yam, J. W. P. (2013). PKA-induced dimerization of the RhoGAP DLC1 promotes its inhibition of tumorigenesis and metastasis. *Nat. Commun.* **4**, 1618. doi:10.1038/ncomms2604
- Korff, T. and Augustin, H. G. (1999). Tensional forces in fibrillar extracellular matrices control directional capillary sprouting. *J. Cell Sci.* **112**, 3249–3258.
- Kupfer, A., Louvard, D. and Singer, S. J. (1982). Polarization of the Golgi apparatus and the microtubule-organizing center in cultured fibroblasts at the edge of an experimental wound. *Proc. Natl. Acad. Sci. USA* **79**, 2603–2607. doi:10.1073/pnas.79.8.2603
- Lamalace, L., Le Boeuf, F. and Huot, J. (2007). Endothelial cell migration during angiogenesis. *Circ. Res.* **100**, 782–794. doi:10.1161/01.RES.0000259593.07661.1e
- Li, G., Du, X., Vass, W. C., Papageorge, A. G., Lowy, D. R. and Qian, X. (2011). Full activity of the deleted in liver cancer 1 (DLC1) tumor suppressor depends on an LD-like motif that binds talin and focal adhesion kinase (FAK). *Proc. Natl. Acad. Sci. USA* **108**, 17129–17134. doi:10.1073/pnas.1112122108
- Liao, Y.-C. and Lo, S. H. (2008). Deleted in liver cancer-1 (DLC-1): a tumor suppressor not just for liver. *Int. J. Biochem. Cell Biol.* **40**, 843–847. doi:10.1016/j.biocel.2007.04.008
- Lin, Y., Chen, N.-T., Shih, Y.-P., Liao, Y.-C., Xue, L. and Lo, S. H. (2010). DLC2 modulates angiogenic responses in vascular endothelial cells by regulating cell attachment and migration. *Oncogene* **29**, 3010–3016. doi:10.1038/ncr.2010.54
- Lin, C., Yao, E., Zhang, K., Jiang, X., Croll, S., Thompson-Peer, K. and Chuang, P.-T. (2017). YAP is essential for mechanical force production and epithelial cell proliferation during lung branching morphogenesis. *eLife* **6**, e21130. doi:10.7554/eLife.21130
- Martin, M., Veloso, A., Wu, J., Katrukha, E. A. and Akhmanova, A. (2018). Control of endothelial cell polarity and sprouting angiogenesis by non-centrosomal microtubules. *eLife* **7**, e33864. doi:10.7554/eLife.33864
- Mason, D. E., Collins, J. M., Dawahare, J. H., Nguyen, T. D., Lin, Y., Voytki-Harbin, S. L., Zorlutuna, P., Yoder, M. C. and Boerckel, J. D. (2019). YAP and TAZ limit cytoskeletal and focal adhesion maturation to enable persistent cell motility. *J. Cell Biol.* **218**, 1369–1389. doi:10.1083/jcb.201806065
- Meerbrey, K. L., Hu, G., Kessler, J. D., Roarty, K., Li, M. Z., Fang, J. E., Herschkowitz, J. I., Burrows, A. E., Ciccio, A., Sun, T. et al. (2011). The pINDUCER lentiviral toolkit for inducible RNA interference in vitro and in vivo. *Proc. Natl. Acad. Sci. USA* **108**, 3665–3670. doi:10.1073/pnas.1019736108
- Möhl, C., Kirchgessner, N., Schäfer, C., Hoffmann, B. and Merkel, R. (2012). Quantitative mapping of averaged focal adhesion dynamics in migrating cells by shape normalization. *J. Cell Sci.* **125**, 155–165. doi:10.1242/jcs.090746
- Nakajima, H., Yamamoto, K., Agarwala, S., Terai, K., Fukui, H., Fukuhara, S., Ando, K., Miyazaki, T., Yokota, Y., Schmelzer, E. et al. (2017). Flow-dependent endothelial YAP regulation contributes to vessel maintenance. *Dev. Cell* **40**, 523–536.e6. doi:10.1016/j.devcel.2017.02.019
- Nardone, G., Oliver-De, La Cruz, J., Vrbnsky, J., Martini, C., Pribyl, J., Skládal, P., Pešl, M., Caluori, G., Pagliari, S. et al. (2017). YAP regulates cell mechanics by controlling focal adhesion assembly. *Nat. Commun.* **8**, 15321. doi:10.1038/ncomms15321
- Neto, F., Klaus-Bergmann, A., Ong, Y. T., Alt, S., Vion, A.-C., Szymborska, A., Carvalho, J. R., Hollfinger, I., Bartels-Klein, E., Franco, C. A. et al. (2018). YAP and TAZ regulate adherens junction dynamics and endothelial cell distribution during vascular development. *eLife* **7**, e31037. doi:10.7554/eLife.31037
- Panciera, T., Azzolin, L., Cordenonsi, M. and Piccolo, S. (2017). Mechanobiology of YAP and TAZ in physiology and disease. *Nat. Rev. Mol. Cell Biol.* **18**, 758–770. doi:10.1038/nrm.2017.87
- Potente, M., Gerhardt, H. and Carmeliet, P. (2011). Basic and therapeutic aspects of angiogenesis. *Cell* **146**, 873–887. doi:10.1016/j.cell.2011.08.039
- Qian, X., Li, G., Asmussen, H. K., Asnaghi, L., Vass, W. C., Braverman, R., Yamada, K. M., Popescu, N. C., Papageorge, A. G. and Lowy, D. R. (2007). Oncogenic inhibition by a deleted in liver cancer gene requires cooperation between tensin binding and Rho-specific GTPase-activating protein activities. *Proc. Natl. Acad. Sci. USA* **104**, 9012–9017. doi:10.1073/pnas.0703033104
- Ritchey, L., Ha, T., Otsuka, A., Kabashima, K., Wang, D., Wang, Y., Lowy, D. R. and Tosato, G. (2019). DLC1 deficiency and YAP signaling drive endothelial cell contact inhibition of growth and tumorigenesis. *Oncogene* **38**, 7046–7059. doi:10.1038/s41388-019-0944-x
- Sánchez-Martín, D., Otsuka, A., Kabashima, K., Ha, T., Wang, D., Qian, X., Lowy, D. R. and Tosato, G. (2018). Effects of DLC1 Deficiency on endothelial cell contact growth inhibition and angiosarcoma progression. *J. Natl. Cancer Inst.* **110**, 390–399. doi:10.1093/jnci/djx219
- Schimmel, L., van der Stoep, M., Rianna, C., van Stalborch, A.-M., de Ligst, A., Hoogenboezem, M., Tol, S., van Rijssel, J., Szulcek, R., Bogaard, H. J. et al. (2018). Stiffness-induced endothelial DLC-1 expression forces leukocyte spreading through Stabilization of the ICAM-1 adhesome. *Cell Rep.* **24**, 3115–3124. doi:10.1016/j.celrep.2018.08.045
- Shih, Y.-P., Takada, Y. and Lo, S. H. (2012). Silencing of DLC1 upregulates PAI-1 expression and reduces migration in normal prostate cells. *Mol. Cancer Res.* **10**, 34–39. doi:10.1158/1541-7786.MCR-11-0450
- Shih, Y.-P., Yuan, S. Y. and Lo, S. H. (2017). Down-regulation of DLC1 in endothelial cells compromises the angiogenesis process. *Cancer Lett.* **398**, 46–51. doi:10.1016/j.canlet.2017.04.004
- Soiné, J. R. D., Brand, C. A., Stricker, J., Oakes, P. W., Gardel, M. L. and Schwarz, U. S. (2015). Model-based traction force microscopy reveals differential tension in cellular actin bundles. *PLoS Comput. Biol.* **11**, e1004076. doi:10.1371/journal.pcbi.1004076
- Szymborska, A. and Gerhardt, H. (2018). Hold me, but not too tight—endothelial cell–cell junctions in angiogenesis. *Cold Spring Harb. Perspect. Biol.* **10**, a029223. doi:10.1101/cshperspect.a029223
- Totaro, A., Panciera, T. and Piccolo, S. (2018). YAP/TAZ upstream signals and downstream responses. *Nat. Cell Biol.* **20**, 888–899. doi:10.1038/s41556-018-0142-z
- Tripathi, V., Popescu, N. C. and Zimonjic, D. B. (2012). DLC1 interaction with α -catenin stabilizes adherens junctions and enhances DLC1 antioncogenic activity. *Mol. Cell Biol.* **32**, 2145–2159. doi:10.1128/MCB.06580-11
- Valent, E. T., van Nieuw Amerongen, G. P., van Hinsbergh, V. W. M. and Hordijk, P. L. (2016). Traction force dynamics predict gap formation in activated endothelium. *Exp. Cell Res.* **347**, 161–170. doi:10.1016/j.yexcr.2016.07.029
- van Buul, J. D., Geerts, D. and Huvemans, S. (2014). Rho GTPases and GEFs: controlling switches in endothelial cell adhesion. *Cell Adh. Migr.* **8**, 108–124. doi:10.4161/cam.27599
- Van Geemen, D., Smeets, M. W. J., Van Stalborch, A. M. D., Woerdeman, L. A. E., Daemen, M. J. A. P., Hordijk, P. L. and Huvemans, S. (2014). F-actin-anchored focal adhesions distinguish endothelial phenotypes of human arteries and veins. *Arterioscler. Thromb. Vasc. Biol.* **34**, 2059–2067. doi:10.1161/ATVBAHA.114.304180
- Vassilev, A., Kaneko, K. J., Shu, H., Zhao, Y. and DePamphilis, M. L. (2001). TEAD/TEF transcription factors utilize the activation domain of YAP65, a Src/Yes-associated protein localized in the cytoplasm. *Genes Dev.* **15**, 1229–1241. doi:10.1101/gad.888601
- Wang, K.-C., Yeh, Y.-T., Nguyen, P., Limqueco, E., Lopez, J., Thorossian, S., Guan, K.-L., Li, Y.-S. J. and Chien, S. (2016a). Flow-dependent YAP/TAZ activities regulate endothelial phenotypes and atherosclerosis. *Proc. Natl. Acad. Sci. USA* **113**, 11525–11530. doi:10.1073/pnas.1613121113
- Wang, L., Luo, J.-Y., Li, B., Tian, X. Y., Chen, L.-J., Huang, Y., Liu, J., Deng, D., Lau, C. W., Wan, S. et al. (2016b). Integrin-YAP/TAZ-JNK cascade mediates atheroprotective effect of unidirectional shear flow. *Nature* **540**, 579. doi:10.1038/nature20602
- Wang, X., Freire Valls, A., Schermann, G., Shen, Y., Moya, I. M., Castro, L., Urban, S., Solecki, G. M., Winkler, F., Riedemann, L. et al. (2017). YAP/TAZ orchestrate VEGF signaling during developmental angiogenesis. *Dev. Cell* **42**, 462–478.e7. doi:10.1016/j.devcel.2017.08.002
- Webb, D. J., Parsons, J. T. and Horwitz, A. F. (2002). Adhesion assembly, disassembly and turnover in migrating cells – over and over and over again. *Nat. Cell Biol.* **4**, E97–E100. doi:10.1038/ncb0402-e97
- Wong, C.-M., Lee, J. M.-F., Ching, Y.-P., Jin, D.-Y. and Ng, I. O. (2003). Genetic and Epigenetic Alterations of DLC-1 gene in hepatocellular carcinoma. *Cancer Res.* **63**, 7646–7651.
- Yu, F.-X. and Guan, K.-L. (2013). The Hippo pathway: regulators and regulations. *Genes Dev.* **27**, 355–371. doi:10.1101/gad.210773.112
- Zacharchenko, T., Qian, X., Goult, B. T., Jethwa, D., Almeida, T. B., Ballestrin, C., Critchley, D. R., Lowy, D. R. and Barsukov, I. L. (2016). LD motif recognition by Talin: structure of the Talin-DLC1 complex. *Structure* **24**, 1130–1141. doi:10.1016/j.str.2016.04.016
- Zhang, L., Yang, S., Chen, X., Stauffer, S., Yu, F., Lele, S. M., Fu, K., Datta, K., Palermo, N., Chen, Y. et al. (2015). The Hippo pathway effector YAP regulates motility, invasion, and castration-resistant growth of prostate cancer cells. *Mol. Cell Biol.* **35**, 1350–1362. doi:10.1128/MCB.00102-15
- Zhao, B., Wei, X., Li, W., Udan, R. S., Yang, Q., Kim, J., Xie, J., Ikenoue, T., Yu, J., Li, L. et al. (2007). Inactivation of YAP oncoprotein by the Hippo pathway is involved in cell contact inhibition and tissue growth control. *Genes Dev.* **21**, 2747–2761. doi:10.1101/gad.1602907
- Zhao, B., Ye, X., Yu, J., Li, L., Li, W., Li, S., Yu, J., Lin, J. D., Wang, C.-Y., Chinnaiyan, A. M. et al. (2008). TEAD mediates YAP-dependent gene induction and growth control. *Genes Dev.* **22**, 1962–1971. doi:10.1101/gad.1664408

Table S1. GEO accession numbers for data analyzed in this study

TEAD1 – muscle : GSM1331246 (RD HUMAN TEAD-CHIPSEQ_48240-treat)

TEAD1 – astrocyte : GSM1515741 (TEAD1-SF268_REP1_54611_treat)

TEAD1 – lung : GSM1664955 (MSTO TEAD1_56535_treat)

TEAD1 – carcinoma : GSM11667161 (HUCCT1 TEAD1_56542_Treat)

H3K4me1 (HUVEC) – GSM733690 (BERNSTEIN_HUVEC_H3K4ME1_45367_treat)

H3K4me3 (HUVEC) – GSM733673 (BERNSTEIN_HUVEC_H3K4ME3_45376_treat)

H3K27ac (HUVEC) – GSM733691 (BERNSTEIN_HUVEC_H3K27AC_45360_treat)

Supplemental Figure 1

TEAD1 interaction with DLC1 enhancer

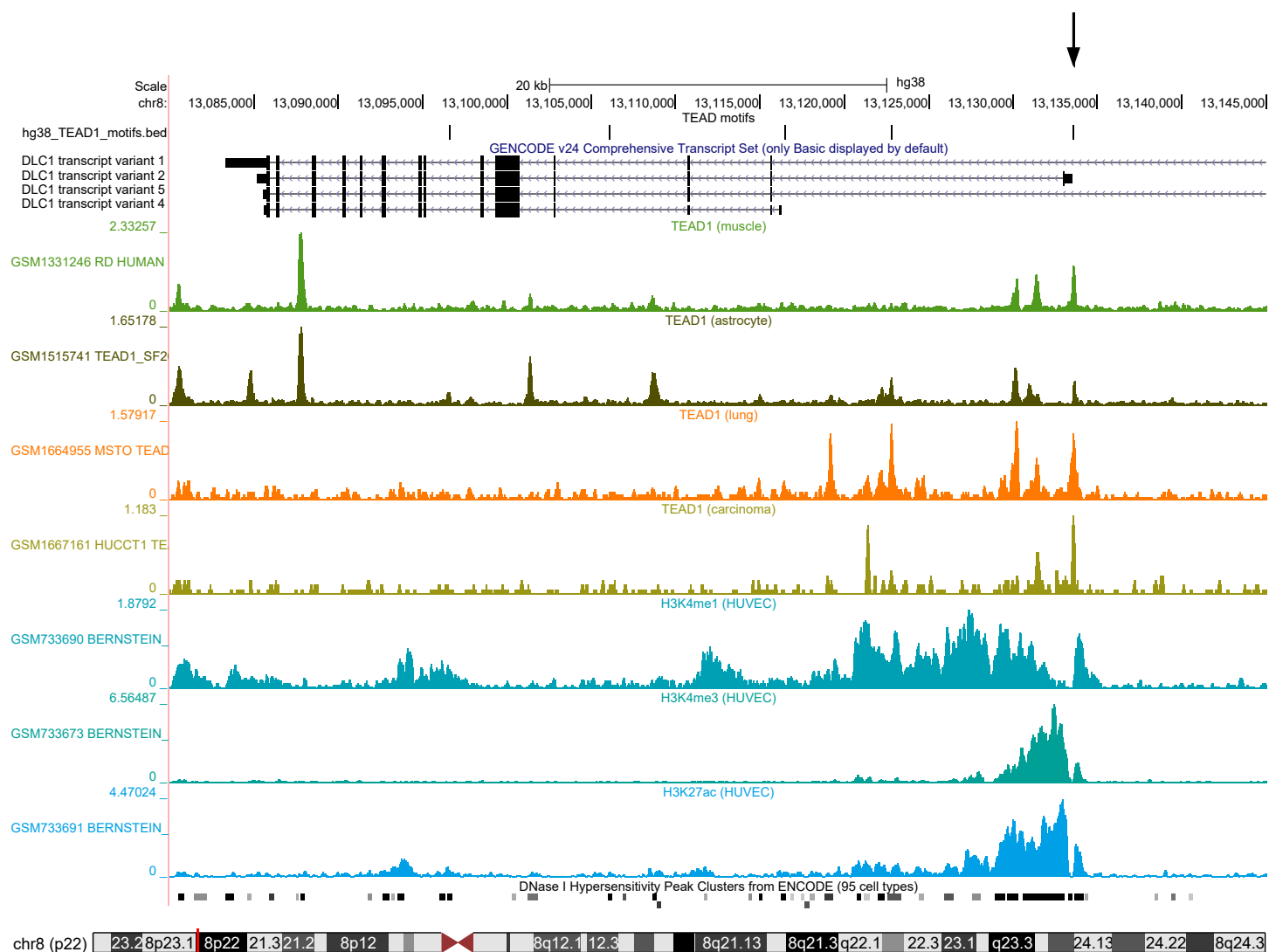


Figure S1. Full detailed schematics of UCSC genome browser results at position chr8:13,074,715-13,142,890 of the human genome (GRCh38/hg38) showing the genomic location of DLC1 transcript variants 1 (NP_872584.2), 2 (NP_006085.2), 5 (NP_001303597.1) and 4 (NP_001157743.1) and the presence of a TEAD motif at the transcriptional start site (TSS) of DLC1 transcript variant 2. Plotted are the results from publicly available GEO data TEAD1 ChIP-Seq data from various cell types and corresponding histone modification profiles in HUVECs in ENCODE. The data show a binding peak of TEAD1 at the TSS of DLC1 transcript variant 2. Histone modification profiles indicate that there is an open conformation of chromatin and an active promoter region around the TEAD binding motif, defined as the bimodal presence of both histone H3 trimethylation at lysine 4 (H3K4me3) and histone H3 acetylation at lysine 27 (H3K27ac), combined with increased DNase hypersensitivity.

Figure S2. Full scans of Western experiments in Figure 1. Molecular weights of the marker, exposure times, sensitive scanning mode and following order of antibody probing are indicated.

Supplemental Figure 2

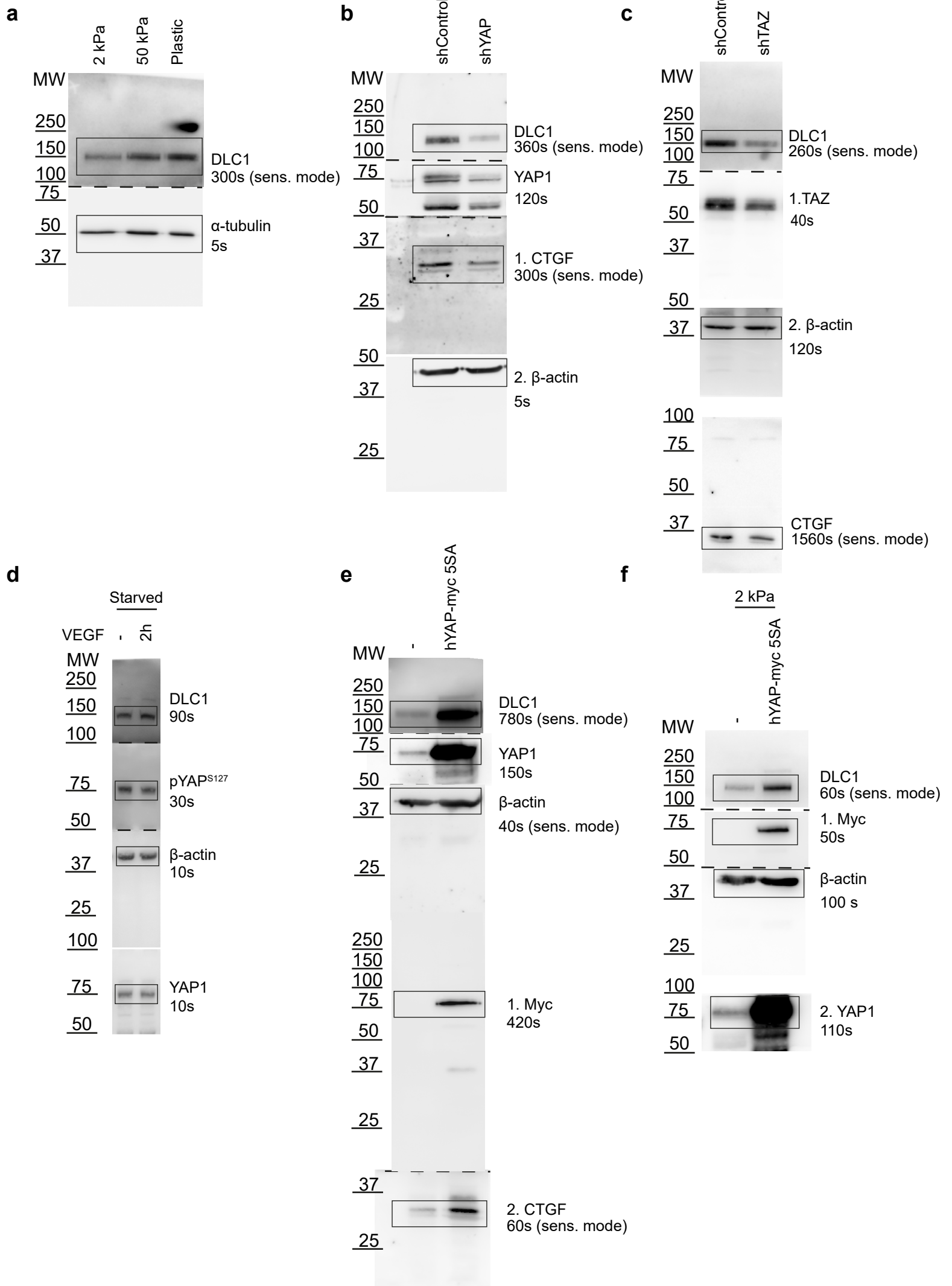


Figure S2. Full scans of Western experiments in Figure 1. Molecular weights of the marker, exposure times, sensitive scanning mode and following order of antibody probing are indicated.

Supplemental Figure 3

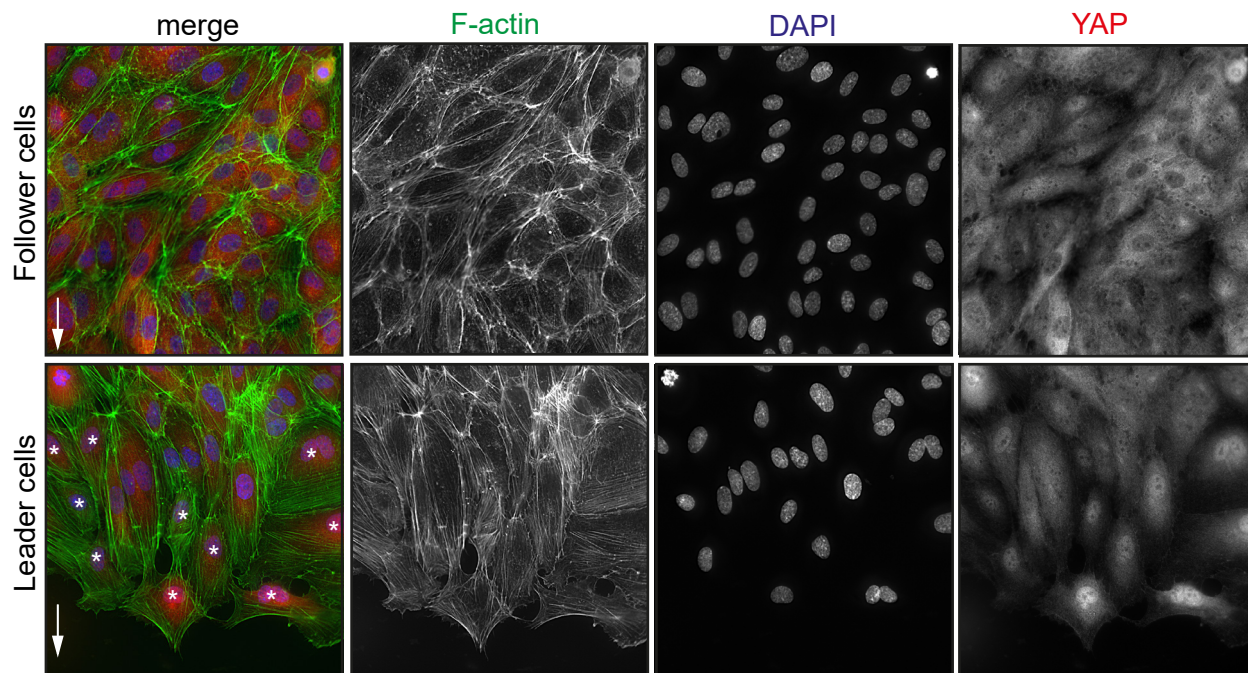


Figure S3. Widefield IF images of HUVECs fixed 6 hours after initiation of scratch wound assays stained for DAPI (blue), F-actin (green) and YAP (red). Pictures taken of the follower cells in the center of the monolayer and of the leader cells at the scratch wound edge. Asterisks highlight cells with nuclear enrichment of YAP compared to the cytoplasm.

Supplemental Figure 4

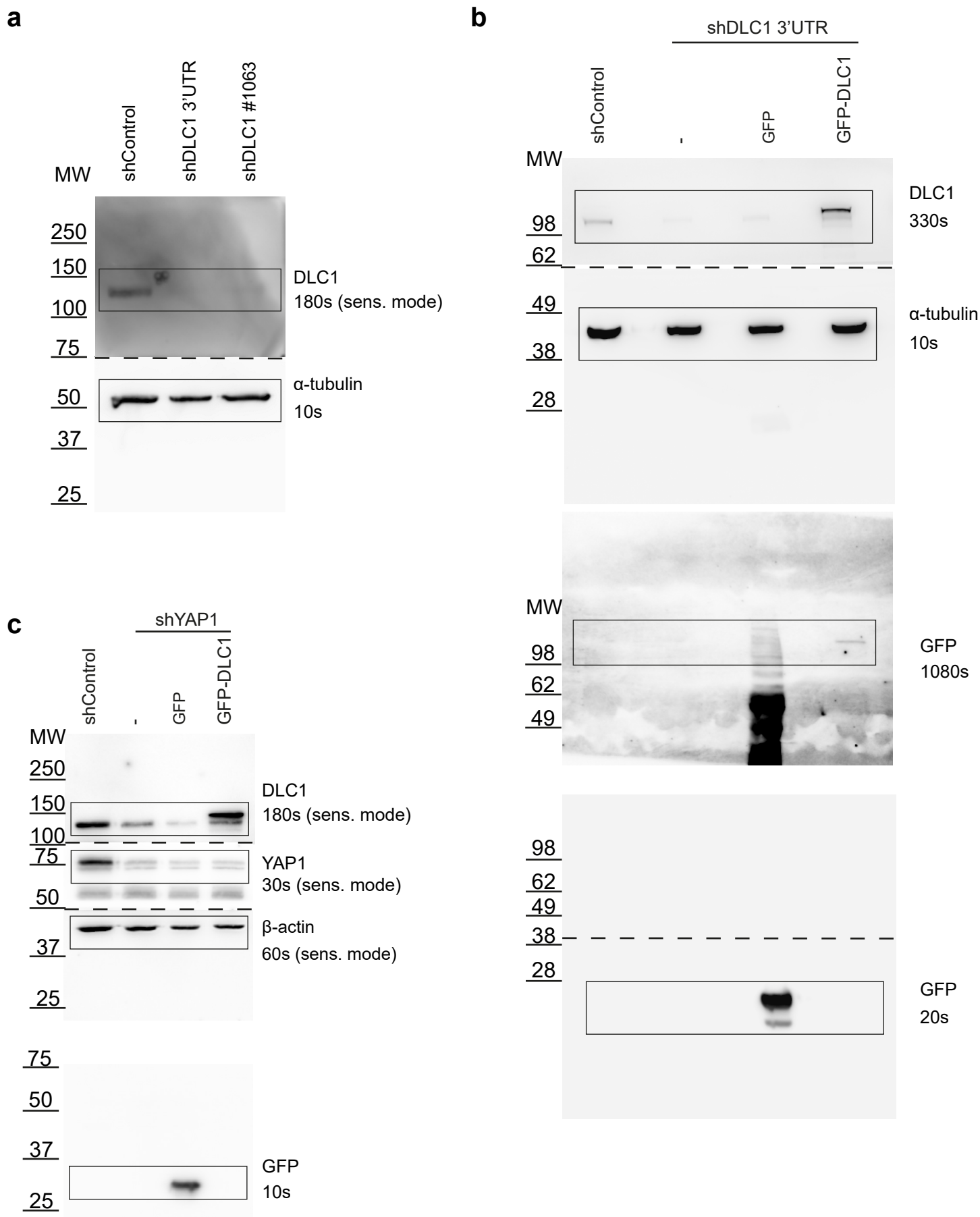
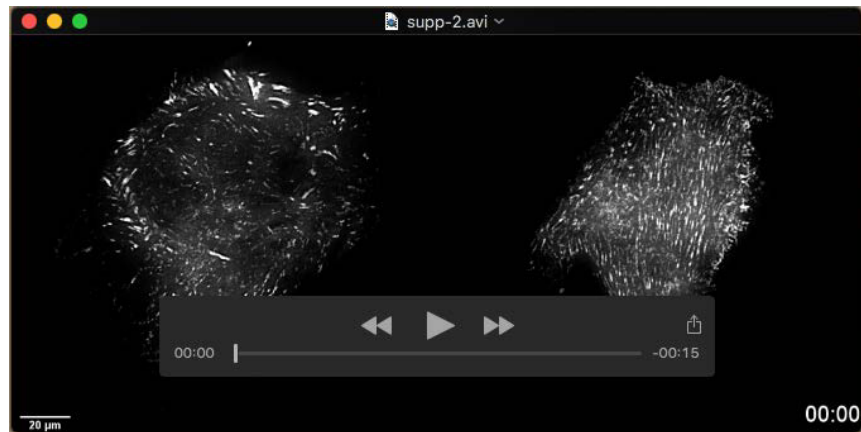


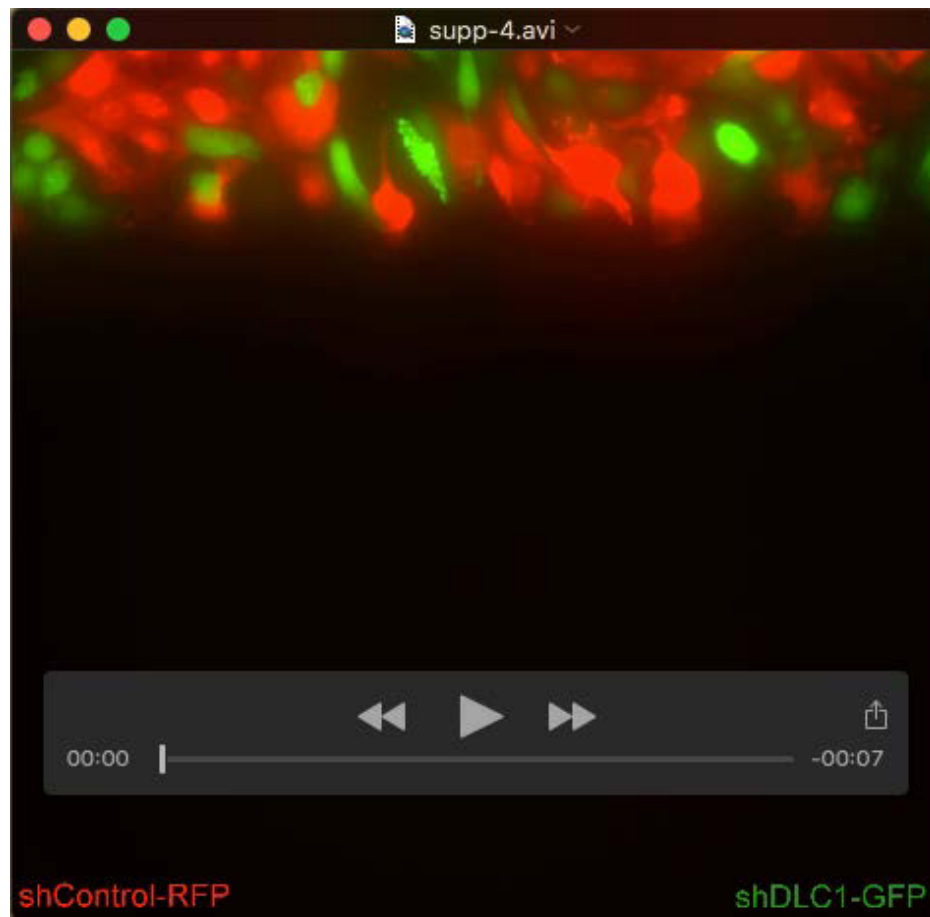
Figure S4. Full scans of Western experiments in Figure 3-5. Molecular weights of the marker, exposure times, sensitive scanning mode and following order of antibody probing are indicated.



Movie 1. DLC1 controls endothelial focal adhesion dynamics. Time lapse recording of HUVECs transduced with shControl or shDLC1 and expressing paxillin-mCherry. Images were acquired by time-lapse TIRF microscopy (NIKON Eclipse Ti) using a 60x/1.49 NA oil objective. Frames were taken every 30 sec for ~ 2,5 hours.



Movie 2. DLC1 is needed for endothelial directional migration. Time lapse recording of HUVECs transduced with shControl, shDLC1 3'UTR or shDLC1 #1063 during scratch wound migration. Images were acquired by time-lapse phase-contrast microscopy (NIKON Eclipse Ti) using a 10x dry objective. Frames were taken every 10 min for ~ 16 hours.



Movie 3. DLC1 is needed to establish leader cells during directional migration. Time lapse recording of mosaic cultures of HUVECs transduced with shControl (RFP) or shDLC1 (GFP) during scratch wound migration. Images were acquired by time-lapse fluorescence microscopy (NIKON Eclipse Ti) using a 20x/0.75 NA dry objective. Frames were taken every 10 min for ~ 17 hours.